Journal of Naval Architecture and Marine Engineering
January, 2026
https://dx.doi.org/10.3329/jname.v23i1.81886 *https://www.banglajol.info*

THERMAL DAMAGE ANALYSIS OF APPLYING SINGLE- AND DOUBLE-SLOT MICROWAVE COAXIAL ANTENNAS FOR TREATING OBLATE, PROLATE, AND CIRCULAR LIVER TUMORS

Chaity Biswas, Rehena Nasrin*, Salma Jahan, and Most. Zannatul Ferdoushi
Department of Mathematics, Bangladesh University of Engineering and Technology, Dhaka, Bangladesh. *Correspondence: rehena@math.buet.ac.bd

Abstract:

*Microwave coaxial antennas (MCA) are essential for effective liver tumor treatment using microwave ablation (MWA). Their configuration significantly impacts the procedure's success by ensuring precise energy delivery, efficient heating, and uniform temperature distribution. This enhances the overall efficacy and security of the medical treatment, leading to improved clinical outcomes and better patient care. In developing an MWA system, the geometric features of the microwave antenna construction must be taken into account. This research examined the effectiveness of single- and double-slot antennas in prolate, oblate, and spherical tumor tissues. The primary goal of this investigation was to modify MWA procedures to achieve complete tumor ablation while minimizing thermal damage to adjacent healthy tissue. An MCA is inserted into liver tissue shaped like a cylinder (length 8 cm, radius 3 cm). The tissue contains a prolate ellipsoidal tumor (2.4 cm * 3.2 cm) and an oblate ellipsoidal tumor (3.2 cm * 2.4 cm). The antenna axis is selected to align with the prolate tumor's central axis and the oblate tumor's minor axis. In this simulation, we are investigating the impact of varying microwave power (6 to 24 W), frequency (600 to 3500 MHz), and time (1 to 450s) on prolate and oblate tumor cells. We are using a finite element method (FEM)-based numerical approach to assess the effectiveness of antennas. The specific absorption rate (SAR) values obtained with a double-slot antenna are significantly higher for various tumor shapes, including circular (6020.87 W/kg), oblate (6004.54 W/kg), and prolate (3099.50 W/kg), than those obtained with a single-slot antenna. Our findings show that with sufficient input power and frequency, necrotic tissue is mainly confined to the tumor, causing minimal thermal damage to surrounding healthy tissue. Interestingly, our results demonstrate that double-slot antennas provide improved localization of thermal damage and enhanced treatment safety compared to single-slot configurations.*

Keywords: MWA; MCA; liver tissue; electromagnetic wave model; bioheat transfer; FEM.

NOMENCLATURE:

Symbols	Designation	Symbols	Designation
C	Heat capacity of specific heat, [J/kg/°C]	P	Microwave input power, [W]
E	Strength of electric field, [V/m]	Q_{ext}	Source of external heat, [W/m^3]
f	Microwave frequency, [Hz]	r	Dielectric radius, [m]
H	Strength of magnetic field, [A/m]	T	Temperature, [°C]
K	Propagation constant, [m^{-1}]	t	Time, [s]
k_0	Propagation constant of free space, [m^1]	Z	Wave impedance of the dielectric cable, [Ω]
K	Thermal conductivity, [W/m°C]		
Greek symbol			
ρ	Density, [kg/m^3]	ϵ	Permittivity, [F/m]
λ	Wavelength, [m]	σ	Electric conductivity, [S/m]
ω	Frequency of angular motion, [rad/s]	μ	Permeability, [H/m]
ω_b	Perfusion rate, [1/s]	Γ	Reflection coefficient

1813-8535 (Print), 2070-8998 (Online) Received: August, 2025

Subscript

b	blood	R	Relative
Ext	External	0	Free space
Met	Metabolic		

Abbreviation

FEM	Finite element method	MWA	Microwave ablation
MF	Microwave frequency (Hz)	RF	Radiofrequency
MP	Microwave power (W)	RFA	Radiofrequency ablation
MW	Microwave	SAR	Specific absorption rate (W/kg)
MCA	Microwave coaxial antenna	TEF	Transverse electromagnetic field
MRI	Magnetic resonance imaging	TEM	Transverse electromagnetic
MTA	Microwave thermosphere ablation		

1. Introduction

The most common causes of death worldwide are cancerous tumors in the lungs, bones, kidneys, liver, breast, and other body parts. The liver is responsible for several essential functions, including filtering toxins and waste products from the bloodstream and preparing them for digestion. Several heating sources are available for the thermal therapy of less invasive cancers. Microwave heating for cancer treatment has attracted significant attention. Patients who are not physically acceptable for surgery or have tumors with a diameter of less than 1.5 inches may consider microwave liver ablation as a potential substitute for therapy.

For men, liver cancer ranks 5th in terms of frequency of occurrence, whereas for women, it ranks 9th. Microwave ablation is a common treatment for hepatocellular carcinoma worldwide. Dielectric measurements were investigated by Schepps and Foster (1980) on soft tumors and healthy tissues over the frequency range of 0.01 to 17 GHz at human body temperature. Researchers present empirical formulas for various soft tissues in this broad frequency range to estimate dielectric characteristics. An axisymmetric electromagnetic model implemented in FEMLABTM 3.0 was used by Bertram *et al*. (2006) to quickly and accurately simulate an MWA antenna. The simulation was proposed as an optimal method for assessing SAR patterns and the reflection coefficient of the applicator used in hepatic MWA. These two measures are often used to assess the performance of such antennas. Yang *et al*. (2007) proposed a new technique for studying high-temperature tissue ablation 2007 by employing an enlarged bioheat diffusion equation. Using FEM and the Bayesian VNSP method, Prakash *et al*. (2008) improved the layout of a floating sleeve antenna for MWA of hepatic malignancies. Incorporating a stochastic element, they considered the inherent variance in the physical characteristics of liver tumors and tissue between people. Santos *et al*. (2009) developed a reliable probabilistic technique for hepatic RF ablation. Using this technique, they were able to statistically assess how the uncertainty of the ablation zone's size was affected by four distinct thermal-electrical characteristics of liver tissue: specific heat, electrical conductivity, blood perfusion, and thermal conductivity.

Chang (2010) investigated three popular techniques for predicting tissue damage. The author found that lesion depth and width are insufficient to describe the treatment volume of multi-tine ablation equipment. Keangin *et al*. (2011) used single- and double-slot microwave coaxial antennas to analyze electromagnetic wave propagation and its thermal exchange in liver MWA. They demonstrated that, with a single-slot antenna, the high-specific absorption rate and temperature occur in liver tissue, and that these values are higher than with a double-slot antenna. Lopresto *et al*. (2012) conducted a numerical study to investigate changes in tissue dielectric properties. They observed a 20% decrease in SAR and an 8% longer thermal lesion with the mineral trioxide aggregate (MTA) treatment. The temperature curves and ablation zones in ex vivo hog livers were compared by Sun et al. (2012) using a microwave ablation and thermal monitoring system operating at 915 and 2450 MHz. The researcher discovered that in ex vivo porcine livers, a 915 MHz cooled-shaft antenna may generate a substantially wider ablation zone and attain higher temperatures within it than a 2450 MHz cooled-shaft antenna. Guntur *et al*. (2013) examined the ex vivo thermal properties of swine liver after heating from 20°C to 90°C and subsequently cooling to 20°C. They proposed that the thermal parameters were insensitive to temperature and maintained nearly constant values throughout tissue cooling, suggesting that their relationship with temperature was unchanging.

Rattanadecho *et al*. (2013) analyzed the MWA technique in a liver with two layers of porous tissue. They used both a single-slot MCA and a double-slot coaxial antenna. Their findings revealed that the double-slot MCA produced a larger ablation area in the porous liver, with two distinct hot-spot zones near the double slots. Viglianti *et al*. (2014) numerically evaluated thermal damage. The simulation was performed on the skin surface, and

exposure temperatures ranged from 60 to 90°C, with each surface temperature held constant for 10 to 110 seconds. They discovered that the cell survival/CEM43 (Cumulative equivalent minutes at 43°C) association for the examples reviewed here most closely corresponds to isothermal tissue exposure at ∼50°C. Acikgoz and Turer (2014) developed a novel T-ring-shaped structure to improve the performance of an MCA for treating liver cancer. The researchers discovered that their novel MCA had a larger localized SAR distribution at the slot location than the conventional one. Additionally, the T-ring-shaped structure of the new MCA resulted in a shorter heating period, accelerating the ablation procedure. Wang et al. (2015) investigated the effectiveness of a novel multi-slot antenna for microwave ablation of malignancies. They found that the coaxial multi-slot antenna significantly reduced over-treatment compared to the traditional one. Additionally, they found that for irregularly shaped tumors, coaxial-slot antennas with different numbers of slots yielded the best results. Curto *et al.* (2015) used an objective method to compare the variations in MCA at 2.45 GHz and 915 MHz. Compared to 915 MHz, theoretical, analytical, and practical studies showed that using a single insulated microwave antenna at 2.45 GHz with 30 W of power at the antenna port resulted in greater power deposition and broader ablation zones.

Wu *et al*. (2016) used a FEM coupled with electromagnetic field and bioheat transfer equations to investigate the impact of high microwave frequencies (6-18 GHz) for liver cancer treatment compared with standard microwave (MW) frequencies (915 MHz, 2450 MHz). Their findings demonstrate that, compared to traditional MWA, high-frequency MWA may result in reduced collateral damage, a more focused ablation zone, and improved material responsiveness. The dependability of a multiphysics dynamic simulation model created for MTA therapy was examined by Lopresto *et al*. (2017) They contrasted numerical data with results from MTA tests carried out on ex vivo bovine liver tissue at 2.45 GHz for ten minutes at a strength of 60 W. Lopresto *et al*. (2017) explored clinical gaps and the latest research advice on MTA for tumor therapy. Analyzing the data, they found that numerical treatment planning should not require advanced computing resources. Jiang *et al*. (2017) examined the effectiveness of novel tri- and single-slot antennas operating at 433 MHz in ex vivo liver tissue. It was found that the existing tri-slot antenna can simultaneously perform multiple-point ablations and cover a larger MWA region. In comparison, the intended single-slot antennas could cover a wider area of the MWA than an antenna operating at 2450 MHz. Deshazer *et al*. (2017) conducted a study comparing experimental measurements with computer simulations of MWA heating patterns. They used a commercially available antenna with a well-defined shape. Although tissue temperature and ablation zone dimensions showed reasonable agreement, there were significant differences between the experimental and simulated SAR results.

Farina *et al*. (2018) conducted a study examining three commercially available devices for tissue shrinkage during microwave thermal ablation. They discovered that the device's design affected the ablation outcome. According to the authors, the tissue in the thermally coagulated zone undergoes a dynamic process of shrinkage that directly correlates with tissue temperature. Gas (2018) investigated an S11-parameter multi-slot coaxial antenna with periodic slots operating at 2.45 GHz for conformal microwave thermotherapy of liver tissue. It shows that the multi-slot microwave coaxial antenna's expanding periodic area count significantly influences its impedance matching to malignant tissue, and the technology may have applications in computerized cancer treatment planning. Sung *et al*. (2020) present an updated report on worldwide cancer prevalence, using the global cancer statistics (GLOBOCAN 2020) estimates of cancer incidence and mortality generated by the International Agency for Research on Cancer. In 2040, it is projected that there will be a total of 28.4 million cancer cases worldwide, which represents a 47% increase compared to 2020. Nasrin *et al.* (2020) investigated blood flow inside a stenotic artery using a power-law fluid model. The results of the blood flow simulations indicated that viscosity increased with higher inlet blood velocity and magnetic strength. Polychronopoulos *et al.* (2021) conducted a computational study on magnetic hyperthermia using nanoparticles derived from ellipsoidal animal tumors, which were modeled as equal-volume prolate and oblate spheroids with varied aspect ratios. They discovered that the aspect ratio and the prolateness and oblateness of the ellipsoid tumors all impacted the amount of the necrotic area. Singh *et al.* (2021) used MIMICS 19.0® and 3-Matic 11.0® image segmentation tools to make a three-dimensional model of a woman's breast with a ~1.7 cm irregular tumor. Findings indicate that 1 mm, 2 mm, and 3 mm fringe heating regions (beyond tumor borders) cause 0.09%, 0.21%, and 0.34% thermal damage to healthy tissue (<1%), leading to effective tumor necrosis. Gorman *et al*. (2022) analyzed three power levels (10W, 20W, and 30W) and the effect of the probe's interior coolant flow rate within a three-dimensional numerical model containing a physically accurate human liver. Researchers found that, at an input power of 10W, it took over twice as long to kill 50% of cells in tissue within a one-centimeter radius as at 30W (less than 100s).

Preechaphonkul and Rattanadecho (2022) analyzed 3D heat transfer in a model of liver cancer with a single blood artery during MWA therapy. Researchers found that the temperature at the tumor edge was affected by a nearby blood vessel. Biswas *et al*. (2022) performed a numerical simulation of microwave cancer treatment in a cylindrical liver tissue model with an elliptical tumor. In this experiment, using a microwave input power of 10W

and a frequency of 2.45 GHz for 180 seconds, the average temperature of the tumor cells reached approximately 56.86°C. Radjenovic *et al.* (2022) conducted three-dimensional simulations using a multi-slot microwave coaxial applicator in two malignancies derived from the 3D-IRCADb-01 liver cancer database. Calculations were performed for a 10-slot antenna operating at 2.45 GHz, positioned within tumors in the liver, which the 3D-ICRADb-01 database categorized as 1.07 and 1.03. It showed that axisymmetric calculations are insufficient for estimating the optimal power and time of ablation. To get accurate findings, 3D simulations of the tumor shape are necessary. In a study by Liu et al. (2023), 76 lesions from 26 patients with multifocal liver cancer who underwent 3.0 Tesla (T) magnetic resonance imaging (MRI)-guided microwave treatment at the hospital from April 2020 to 2022 were investigated. Except for a minor amount of pleural effusion and right upper abdomen discomfort, the researchers found no significant consequences like excessive bleeding, liver failure, or infection following the procedure. Singh (2023) proposes a modification to the conventional Pennes bioheat equation by integrating the effects of perfusion heterogeneity through the introduction of a spatially variable perfusion term, denoted as a perfusion coefficient, $\omega_b(x, y, z)$, to account for localized fluctuations in blood flow at each spatial coordinate within the biological tissue.

Waseem *et al*. (2023) numerically analyzed the effects of internal heat production and thermal radiation on heat transfer and temperature distribution within a nanofluid system. Nasrin and Sawmpa (2024) performed a 3D numerical analysis of malignant tumor ablation using an electric current and bioheat transfer model and concluded that tumor cells were effectively destroyed at approximately 50°C using 22 volts over a 480-second heating period. Hossain *et al.* (2025) compared skin burn intensity using a multilayer bioheat transfer model and an Arrhenius damage analysis, showing that the effect of duration was strongly dependent on exposure time and temperature. Thermal radiation and diffusion effects on MHD Sisko fluid flow were analyzed by Adilakshmi *et al.* (2025). Reddy *et al*. (2025) numerically examined the effects of thermal radiation, a magnetic field, and convective boundary conditions on MHD Maxwell nanofluid flow over an expanding surface and found that radiation increases the temperature. Sohail *et al.* (2025) examined bio-convective Maxwell nanofluid flow over a stretched sheet using the optimal homotopy analysis method and demonstrated the significant effects of radiation, fluid relaxation, and Darcy-Forchheimer effects on temperature and skin-friction characteristics. Very recently, Dong *et al* (2025) reviewed recent advancements in microwave ablation as a minimally invasive thermal therapy for tumor treatment. The authors highlighted that, compared with RFA, MWA operates at high frequencies and enabling faster heating rates, larger ablation zones, and reduced sensitivity to tissue impedance.

Based on the information provided, the even distribution of microwave energy is crucial for effective tumor ablation. Antennas with single and double slots exhibit distinct energy distribution patterns that can significantly affect tumor destruction. Researchers strive to optimize tumor ablation while minimizing damage to healthy liver tissue by fine-tuning microwave power and frequency. As far as the author is aware, there are still some areas where scholars may benefit from devoting more attention, such as:

- Research new designs for single- and double-slot antennas to enhance control over energy distribution and penetration depth. This involves considering variations in slot shape, size, and positioning to improve ablation efficacy.
- Conducting a thorough investigation of potential side effects, complications, and mitigation strategies.
- Exploring the impact of different microwave frequencies and modulations to optimize energy absorption by the tumor and minimize damage to healthy tissue.
- Developing more precise heat distribution and tissue interaction models to better anticipate and manage the ablation process.

This study numerically investigates the efficacy of single- and double-slot antennas in treating oblate and prolate liver tumors. The primary objectives of the present study are as follows:

The objectives of this research are:

- Identifying the most effective energy transfer mechanism.
- Adjusting antenna geometry for optimal performance.
- Investigating the effects of MW on various tumor cell shapes.
- Estimating thermal conduction in liver tissue during MWA using single- and double-slot MCA.
- Detecting the optimal MW frequency, power, and time combination that maximizes tumor destruction.
- Conducting a comparative analysis of single- and double-slot MCA regarding MW dissipation density, MW absorption, SAR distribution, thermal damage, thermal energy generation, and temperature distribution.

In microwave cancer therapy for liver tissue, researchers have found that the antenna shape is critical for treating different types of liver tumors. The antenna's shape directly impacts the treatment's effectiveness, precision, and safety. In this study, we aim to understand how tumor shape influences microwave ablation outcomes. Specifically, we ask whether circular, oblate, and prolate liver tumors respond differently to microwave energy, and whether a double-slot antenna can provide more localized heating and better protection of surrounding healthy tissue compared to a single-slot antenna under clinically relevant conditions.

The current work offers a thorough comparison of single- and double-slot microwave coaxial antennas for treating prolate, oblate, and circular liver tumors, in contrast to most previous microwave ablation studies, which consider only simpler or spherical tumor geometries. A fundamental novelty of this work is the insertion of a second slot near the antenna tip within the tumor, which dramatically improves localized heating compared to single-slot setups, regardless of tumor form or size. Additionally, the study shows that the double-slot antenna achieves more concentrated thermal deposition under low-power, high-frequency conditions, thereby improving ablation control and reducing collateral tissue damage. It does this by methodically comparing high-power–low-frequency and low-power–high-frequency operating regimes. Ultimately, the findings provide useful direction for clinical microwave ablation protocols by identifying an ideal operating condition (12 W, 3.5 GHz, 240s) that may successfully ablate tumors with a diameter of 3–4 cm.

2. Graphical Abstract

The graphical abstract depicted in Figure 1 elucidates the modeling of electromagnetic wave applications in tumor treatment. This study compares the efficacy of single- and double-slot antennas for prolate (elongated) and oblate (flattened) tumor morphologies. The findings suggest that double-slot antennas significantly enhance treatment efficiency by concentrating energy within the tumor mass, thereby reducing adverse effects on adjacent healthy tissue.

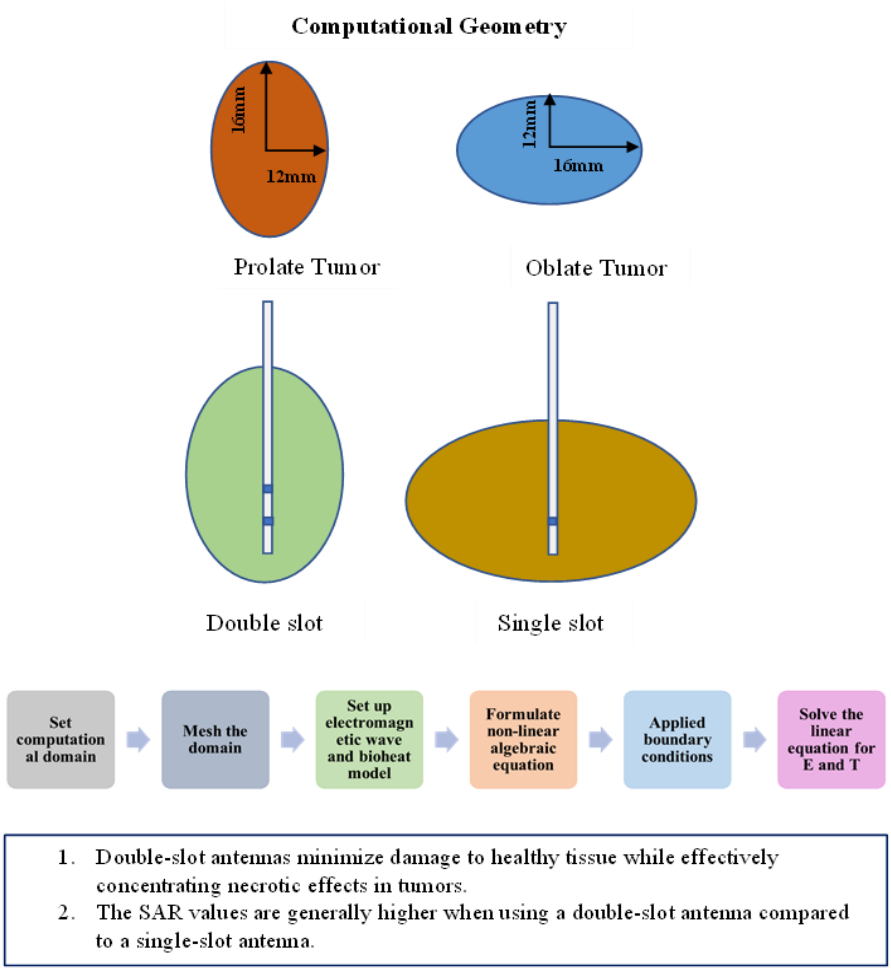

Figure 1: Graphical abstract of the considered model

3. Physical Modeling

An 80 mm-long probe with single- and double-slot configurations was used to efficiently transfer heat from the microwave applicator to the tissue. The liver tissue under consideration is cylindrical, with a radius of 3 centimeters and a length of 8 centimeters, and is surrounded by air. The MCA is inserted into the liver cells at a depth of 71.5 mm. To streamline processing time while preserving excellent resolution and capturing the fields' complete three-dimensional (3D) attributes, an axially symmetric model is adopted for this study. The longitudinal axis of the MCA is aligned with the vertical axis, while the radial direction is aligned with the horizontal axis. Figure 2 visually represents the 3D and two-dimensional (2D) (axisymmetric) physical model.

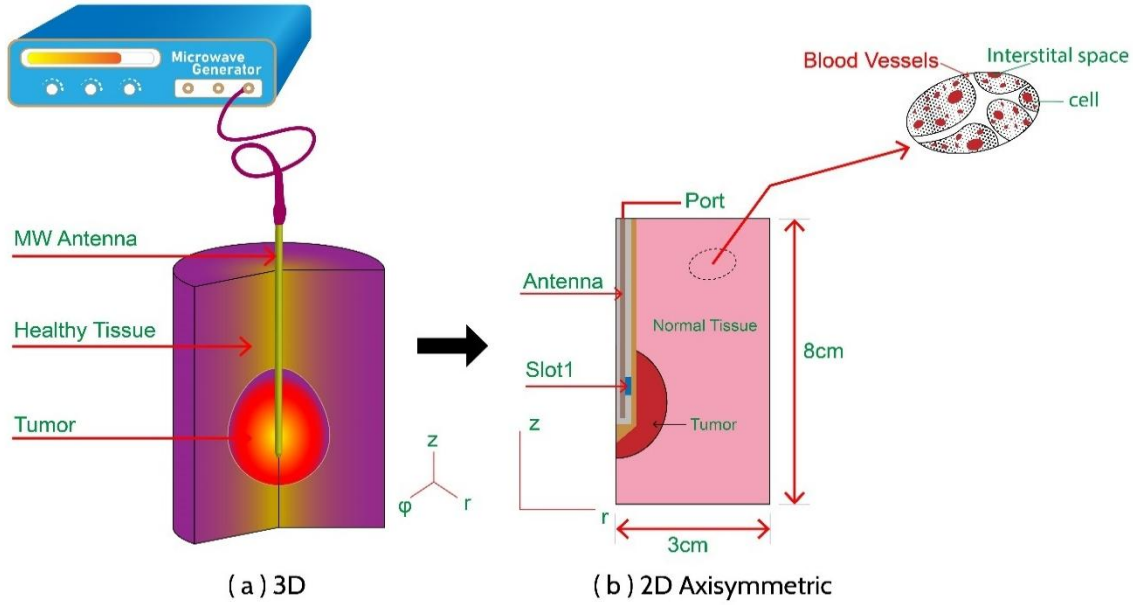

Figure 2: Physical geometry in (a) 3D, and (b) 2D axisymmetric form

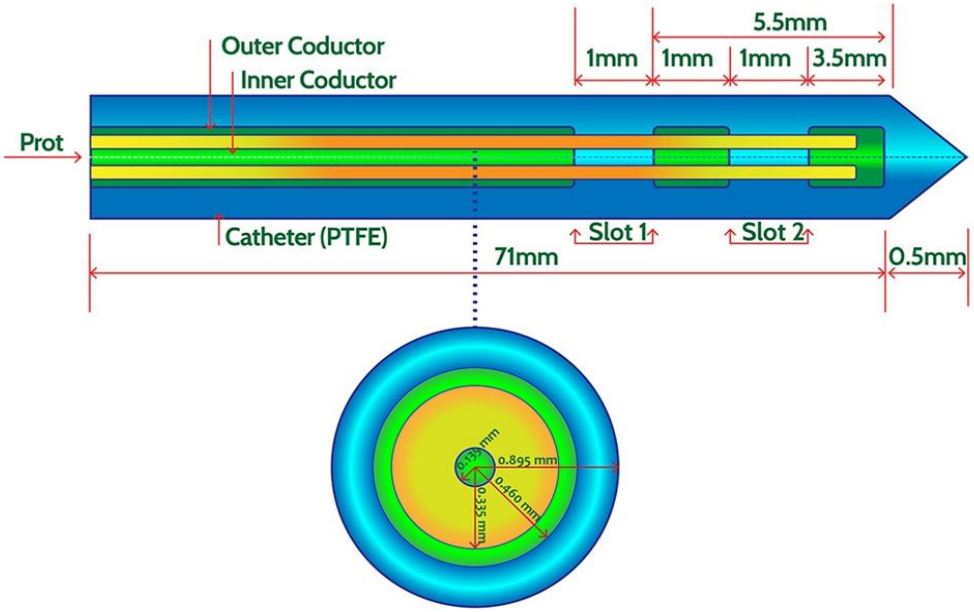

Figure 3: Schematic diagrams illustrating a double-slot antenna's axial and radial components based on a coaxial configuration.

The illustration in Figure 3 presents an innovative single- and double-slot antenna design. The antenna tip has a conductor constructed like an arrow, aiding the smooth insertion into liver tissue. The antenna probe consists of a dielectric material (Teflon) between the inner and outer conductors (copper), as well as a polytetrafluoroethylene

(PTFE) catheter. The slot is 1 mm long, and its position is a critical factor in tumor removal. Our research focuses on analyzing variations in tumor shape, specifically modeling tumors as prolate spheroids with major axes of 24 mm and minor axes of 32 mm, and as oblate spheroids with equal volumes.

This study focuses mainly on ellipsoids, a special instance of perfectly spherical tumors. These forms are often referred to as ellipsoidal due to revolutionary change. In this case, the z-axis is labeled as the rotational axis. Figure 4 displays oblate spheroids with a semi-axis a > b, and prolate spheroids with a semi-axis a < b.

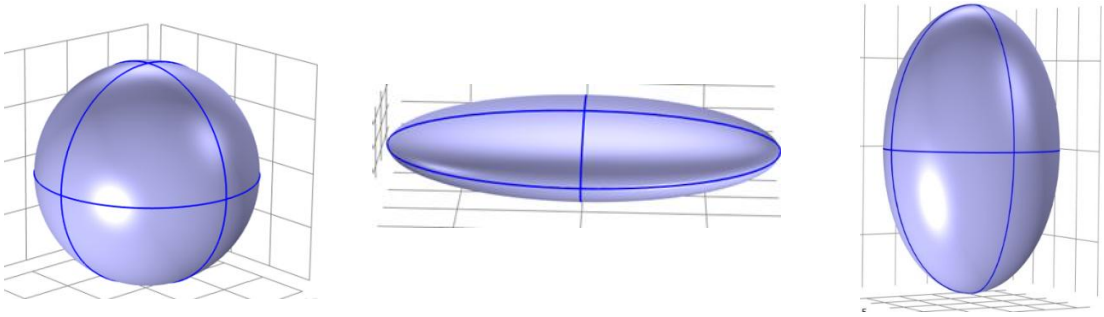

(a) (b) (c)

Figure 4: Virtual representation of tumors (a) circular, (b) oblate, and (c) prolate by ellipsoid geometry.

In the initial set of simulations, all material attributes will be described as homogeneous and isotropic. The permittivity of free space, denoted as ε, is approximately equal to 8.8542×10^{-12} F/m. Similarly, the permeability of free space, denoted as μ_0, is approximately equal to 1.2566×10^{-6} H/m. Gathering material attributes from multiple sources was crucial because no reference contains all the necessary features [Schepps *et al.* (1980), Lopresto *et al*. (2012), Sun *et al*. (2012), Deshazer *et al*. (2017)].

Tables 1-3 contain the material properties of computational geometry, including thermophysical and electromagnetic characteristics for all materials investigated at a frequency of 2.5 GHz.

Table 1: Material properties of liver, antenna, and tumor tissue [Keangin *et al*. (2011), Rattanadecho *et al.* (2013), Biswas *et al.* (2022)].

Material	Amount (mm)
Catheter diameter	1.79
Diameter of the dielectric	0.335
Diameter of the outer conductor	1.19
Diameter of the central conductor	0.29
Height of the slot	1.0
Length of the liver cell	80
Radius of the liver cell	30
The major axis of the tumor	32
The minor axis of the tumor	24
Insertion depth of antenna	71.5

Table 2: Thermophysical properties for the solid materials [Schepps *et al.* (1980), Lopresto *et al*. (2012), Sun *et al*. (2012), Deshazer *et al*. (2017)].

		Density (kg/m^3)	Specific Heat J/(kg·K)	Thermal conductivity (W/m.K)
Tissue	**Liver**	1079	3540	0.52
	Blood	1000	3639	0.49
	Tumor	1050	3500	0.56
Applicator	**Copper**	8960	386	401
	Teflon	800	1000	0.25

Table 3: Properties of electromagnetic waves at 2.45 GHz [Schepps *et al.* (1980), Betram *et al.* (2006), Keangin *et al.* (2011), Lopresto *et al.* (2012), Farina *et al.* (2018), Biswas *et al.* (2022), Tasnim and Nasrin (2024)].

		Relative permittivity ε_r	Relative permeability μ_r	Electric conductivity σ (S/m)
Tissue	**Liver**	43.03	1	1.69
	Blood	58.30	>1	2.54
	Tumor	40.00	1	1.00
Applicator	**Copper**	1.0	0.999	5.8×10^7
	Teflon	1.7	1.000	0

4. Mathematical Modeling

The study introduced MWA into liver tissue using a finite element approach. It analyzed heat distribution within biological tissues using bioheat transfer and electromagnetic wave models. A transverse electromagnetic (TEM) wave, produced by MW generators and transmitted over a coaxial wire, is included in the model. The model and simulation settings were chosen based on practical microwave ablation factors relevant to treating liver tumors. This includes realistic tumor sizes, standard microwave power and frequency ranges, achievable treatment durations, and the aim to maximize tumor destruction while limiting thermal damage to surrounding healthy liver tissue. Antenna configurations were also selected to mirror practical placement and planning considerations.

4.1. Electromagnetic wave model

The governing equation that describes the behavior of electromagnetic waves in liver tissue according to [Preechaphonkul and Rattanadecho (2022), Biswas *et al*. (2022), Andreozzi *et al.* (2024), Tasnim *et al.* (2024)] is:

$$\nabla \times \mu_r^{-1}(\nabla \times \mathbf{E}) - k_0^2(\epsilon_r - \frac{j\sigma}{\omega\epsilon_0})\mathbf{E} = 0 \quad (1)$$

Here, μ_r is the relative permeability, ϵ_r is the relative permittivity, j is the imaginary unit, used here to represent the phase difference between the electric field and the current it induces, σ is the electrical conductivity of the medium (S/m), ω is the angular frequency of the wave (rad/s), free space permittivity is denoted by ϵ_0. k_0 is the wave number in free space, given by:

$$k_0 = \frac{2\pi}{\lambda}$$

where λ is the wavelength.

$\mathbf{E}$ is the electric field vector and is expressed as: $\mathbf{E}(r,\varphi,z) = \mathbf{E}(r,z)e^{-im\varphi}$.

This expression is vital for describing systems with cylindrical symmetry and understanding wave behavior in such systems.

The time-averaged power flow in the cable is expressed as:

$$\mathbf{P}_{av} = \int_{r_{inner}}^{r_{outer}} Re\,(\frac{1}{2}\mathbf{E} \times \mathbf{H}) 2\pi r dr \tag{2}$$

where, electrical field, $\mathbf{E} = e_r \frac{C}{r} e^{j(\omega t - kz)}$, and magnetic field, $\mathbf{H} = e_\varphi \frac{C}{Z} e^{j(\omega t - kz)}$

The cylindrical coordinates r, φ, and z are defined with respect to the axis of the coaxial cable, with z pointing in the direction of propagation. The $\mathbf{P}_{av}$ symbol represents the time-averaged power flow in the cable. Z refers to the wave independence in the dielectric cable, while r_{inner} and r_{outer} represent the inner and outer radius of the dielectric, respectively.

The dielectric characteristics are characterized by two significant parameters: relative permittivity (ϵ) and electrical conductivity (σ) [Lopresto *et al.* (2012), Biswas *et al*. (2022), Tasnim *et al.* (2024)]:

$$\epsilon = \epsilon' - j\epsilon'' = \epsilon' - j\frac{\sigma}{\omega\epsilon_0} \tag{3}$$

ϵ' represents the dielectric constant, whereas ϵ'' is associated with the conductivity of tissue electricity. The input reflection coefficient (S_{11}) and the phase angle θ of the reflection coefficient are used in a capacitance measuring model [Deshazer *et al.* (2017), Singh (2023), Andreozzi *et al.* (2024)] to determine dielectric characteristics:

$$\epsilon' = \frac{1}{\omega z_0 c_0} \frac{-2|\Gamma| sin\theta}{1 + 2|\Gamma| cos\theta + |\Gamma|^2} \tag{4}$$

$$\epsilon'' = \frac{1 - |\Gamma|^2}{-\omega z_0 c_0 (1 + 2|\Gamma| cos\theta + |\Gamma|^2)} \tag{5}$$

$$S_{11} = 20log(\Gamma) \tag{6}$$

In this equation, z_0 represents the coaxial cable's typical impedance (50Ω) and Γ represents the reflection coefficient.

4.2. Bioheat transfer model

Heat transfer in tissue is governed by the Pennes equation, which has been widely utilized to address bioelectromagnetic problems. The Pennes equation is expressed according to [Biswas *et al*. (2022), Nasrin and Sawmpa (2024), Tasnim *et al.* (2024)] as:

$$\rho C \frac{\partial T}{\partial t} + \nabla.(-k\nabla T) = Q_{ext} + Q_{bio} \tag{7}$$

where, ρ is the density of tissue, *C* is the specific heat capacity, k is the thermal conductivity, Q_{ext} represents the external heat source and Q_{bio} can be expressed as [Biswas *et al*. (2022), Nasrin and Sawmpa (2024), Tasnim *et al.* (2024)]:

$$Q_{bio} = \rho_b C_b \omega_b (T_b - T) + Q_{met} \tag{8}$$

where ρ_b represents the blood density, C_b represents the capacity of specific heat, ω_b is the rate of blood perfusion, and the metabolic heat source is represented by Q_{met}.

There is a relationship between the specific absorption rate (SAR) and the external heat source (Q_{ext}), and this relationship is described by [Biswas *et al*. (2022), Nasrin and Sawmpa (2024)]:

$$SAR = \frac{Q_{ext}}{\rho} = \frac{\sigma_{liver}}{2\rho} |\mathbf{E}|^2 \tag{9}$$

Here, **E** is the maximal value of the electric field induced in the liver tissue.

4.3. Thermal damage model

Thermal damage occurs when thermal energy denatures tissue proteins. The study uses the Arrhenius damage model to analyze thermal damage in tumor and normal tissues.

Arrhenius is expressed as [Andreozzi *et al.* (2024)]:

$$\frac{d\alpha}{dt} = A\, e^{(-\frac{\Delta E}{RT})} \tag{10}$$

where A represents the frequency factor (s^{-1}), R is the gas constant (J/mol.K) and $\Delta\mathbf{E}$ is the activation energy (J/mol).

The fraction of necrotic tissue is expressed as:

$$\theta_d = 1 - e^{(-\alpha)}. \tag{11}$$

4.4. Boundary conditions for electromagnetic wave model

Thermal damage occurs when thermal energy denatures tissue proteins. The Arrhenius damage model analyzes thermal damage in both tumor and normal tissue.

- The dielectric, inner, and outer conductor boundaries are considered perfect electric conductors, which is expressed by: $\vec{n} \times \vec{E} = \vec{0}$
- At the port boundary: The S parameter is equivalent to the voltage reflection coefficient Γ [Biswas *et al.* (2022), Nasrin and Sawmpa (2024)].

$$S = \Gamma = \frac{\int(\vec{E} - \overrightarrow{E_1}).\overrightarrow{E_1}}{\int \overrightarrow{E_1}.\overrightarrow{E_1}}$$

In microwave power flow, the voltage reflection coefficient is directly proportional to the ratio of the reflected power (P_r) to the input power (P) at the antenna port. This relationship can be expressed as follows:

$$P = \frac{P_r}{|\Gamma|^2}$$

- When estimating reflections, the area outside of the computational geometry is regarded as a scattering boundary and can be described as

$$\vec{n} \times (\nabla \times \vec{\mathbf{E}}) - jk\vec{\mathbf{n}} \times (\vec{\mathbf{E}} \times \vec{\mathbf{n}}) = \vec{\mathbf{0}}$$

- The interfaces between the liver tissue and tumor tissue are considered as a continuity boundary condition: $\vec{n} \times (\overrightarrow{\mathbf{E}_1} - \overrightarrow{\mathbf{E}_2}) = \vec{0}$
- The axis Z is considered as symmetry conditions: $\mathbf{E}_r(t, r = 0, z)$ and $\frac{\partial \mathbf{E}_z}{\partial r}(t, r = 0, z)$

4.5. Boundary conditions for bioheat transfer wave model

- The initial temperature for the healthy liver tissue domain is considered as $T_0 = 37$℃
- The interfaces between the biological tissue and the MCA are regarded as having a thermally isolated boundary state: $-\vec{n}.\vec{q} = 0$
- The metabolic heat source for liver tissue is $Q_{met} = 1000$ W/m^3
- The metabolic heat source for Tumor tissue is $Q_{met} = 1.3 \times 1000$ W/m^3.

The tumor's metabolic heat generation was assumed to be 1.3 times that of healthy liver tissue to account for the increased metabolic activity and vascularization commonly observed in malignant tissues. This assumption is consistent with Pennes' bioheat model and subsequent microwave ablation studies, which employ elevated metabolic heat values for tumors to reflect enhanced cellular activity and perfusion [Lopresto *et al.* (2017a-b), Rattanadecho and Keangin (2013)].

5. Calculation Procedure

In this study, a numerical analysis is performed using the finite element method (FEM). The computational domain is coupled with electromagnetic wave propagation and bioheat transfer models. The solution model is discretized into a finite number of nonuniform triangular elements. Six electric field-related nodes (**E**) and temperature (T)

are defined for each triangular element. Nonlinear algebraic equations are derived to solve for these unknown variables (**E** and T). In addition, we apply certain boundary conditions to simplify the nonlinear algebraic equation. Then we use Newton's method to convert the nonlinear equation into a linear one. Subsequently, we use the triangular factorization technique to solve these linear equations. The solution procedure's convergence criteria are defined as $|\Psi^{m+1} - \Psi^m| \leq 10^{-6}$, where *m* represents the number of iterations, and Ψ is a function of variables **E** and T. We can refer to [Nasrin *et al.* (2020), Preechaphonkul *et al*. (2022), Biswas *et al*. (2022), Singh (2023), Nasrin and Sawmpa (2024), COMSOL Multiphysics Model Library] for more detailed information on this technique.

5.1 Mesh generation

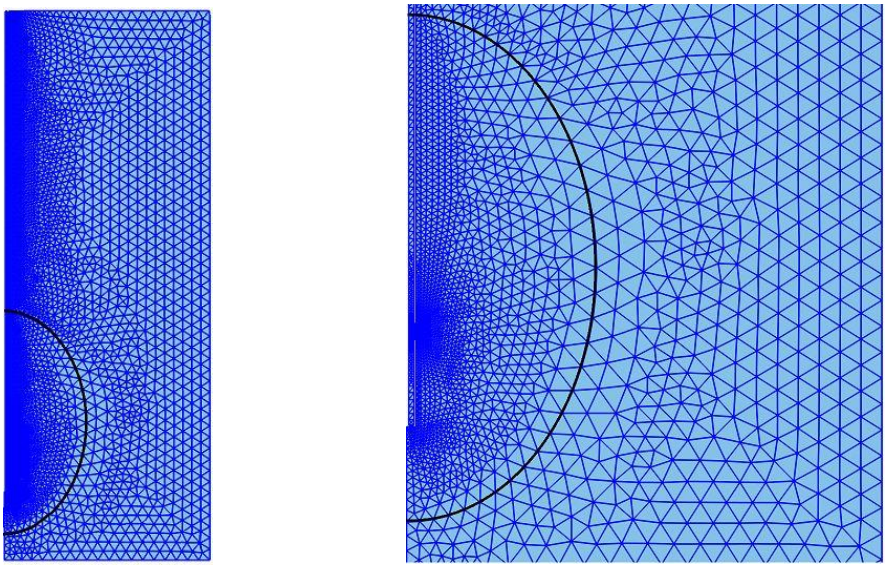

Original view Zoom view

(a) Single-slot antenna within the prolate tumor

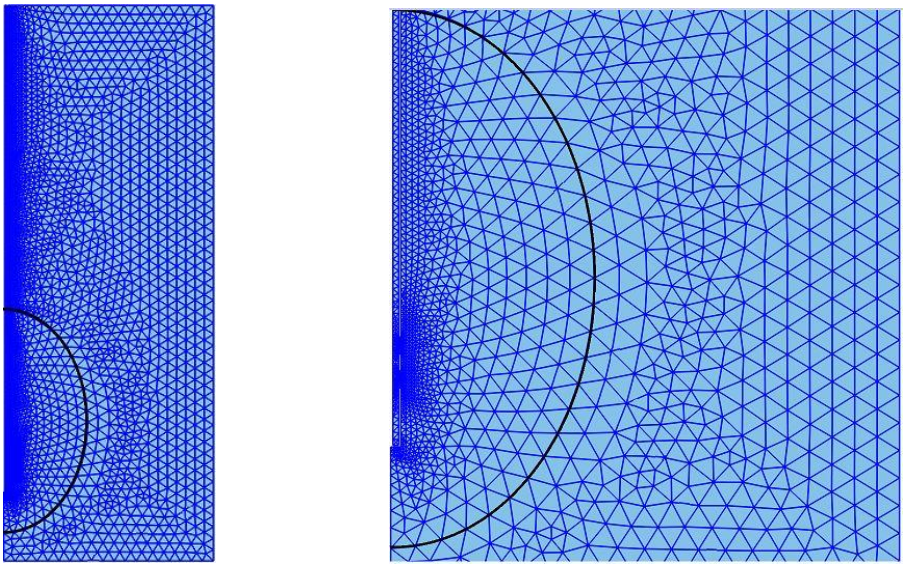

Original view Zoom view

(b) Double-slot antenna within a prolate tumor

Figure 5: Mesh generation of (a) single-slot antenna, and (b) double-slot antenna within the prolate tumor.

Complex geometry is simplified through mesh generation, which involves creating a computational area and dividing the geometry into finite triangular elements. The solution to a problem is directly influenced by several

key variables, including the time required to compute the model, the memory usage during computation, the method used to interpolate the solution between nodes, and the overall efficiency of the solution. In Figure 5(a-b), the FEM meshing of the computational geometry of a prolate tumor with a single-slot and a double-slot MCA is shown. We check five mesh types (normal, fine, finer, extra fine, and extremely fine) at an MW frequency of 3.5 GHz, a power of 12 W, and a time of 240s. We use extra fine meshing for accuracy, with the single-slot antenna having 5486 domain and 833 boundary elements (Figure 5(a)), and the double-slot antenna having 5765 domain and 866 boundary elements (Figure 5(b)).

5.2 Grid checking

Grid sensitivity analysis is performed for four mesh types at f = 3.5 GHz, P = 12 W, and t = 240 s, using liver tissue with the double-slot antenna for the prolate tumor. The optimal value of the SAR is designated as the governing parameter for verifying the accuracy of the numerical solution. Given the acquired SAR values and the required simulation duration, the present simulations are executed using a grid configuration with 14,589 degrees of freedom and 6,631 elements. Table 4 indicates that further improvement in accuracy does not occur with increased degrees of freedom and elements. Similarly, for liver tissue with other tumor shapes and single- and double-slot MCAs, an extra-fine mesh type is chosen for numerical simulation.

Table 4: Grid sensitivity check of the liver tissue with the double-slot antenna of the prolate tumor at f = 3.5 GHz, P = 12 W, and t = 240s

Mesh type	Normal	Fine	Finer	Extra Fine	Extremely Fine
Degrees of freedom	11921	12625	12923	14589	21103
Elements	4822	5014	5538	6631	8395
SAR (W/kg)	3098.2543	3098.7219	3099.1031	3099.5012	3099.5013
Time (s)	21	32	55	69	97

6. Outcomes with Explanations

This study investigates the impacts of varying microwave power (MP) (6 to 24 W) and microwave frequency (MF) (0.6 to 3.5 GHz) over 0 to 450 seconds. The efficacy of single-slot and double-slot antennas in microwave ablation treatments is markedly affected by their design attributes and slot placement. A 1 mm slot on the single-slot antenna is 5.5 mm from the tip. This slot concentrates energy, resulting in fewer necrotic zones and less damage to healthy tissue. However, it is not as good for bigger tumors. The double-slot antenna, with two 1 mm slots separated by 1 mm, the second located 3.5 mm from the tip, enhances energy transmission. This design positions the second slot closer to the tip, concentrating energy on the tumor site, thus boosting necrosis of malignant tissue and minimizing harm to surrounding healthy tissue. The results demonstrate that the double-slot design offers enhanced therapeutic effectiveness and accuracy, overcoming the shortcomings of both single-slot and conventional double-slot designs, thereby establishing it as a preferable option for targeted ablation. The research specifically focuses on the potential harm to healthy tissue due to prolonged exposure to microwave radiation. The simulation results include representations of microwave power dissipation density, transient thermal distribution, and the proportion of damaged tissue.

6.1 Role of MF on total power dissipation density

Microwave frequency (MF) is essential for determining the total power dissipation density (emw) during liver tumor treatment. The frequency chosen influences the depth of penetration, heating patterns, and the overall efficiency of the ablation process. Customizing the frequency based on the specific characteristics of the tumor and surrounding tissues is crucial for achieving optimal treatment outcomes.

The results of computer simulations conducted in the MF range of 0.6 to 3.5 GHz demonstrate the total power dissipation density in liver tissue when P = 12 W and t = 240s are applied. These results are visualized in Figure 6(a-b). Figure 6(a) illustrates the overall power dissipation density in liver tissue using a single-slot antenna, while Figure 6(b) presents the scenario when a double-slot antenna is employed. As the MF increases, the radiated power concentrates around the antenna slot. The image demonstrates the extent of the heating impact that MWA is

expected to have. Near the slot, the dispersion of MP takes on an oval shape and generates a high value. Compared with a single-slot antenna, a double-slot antenna shows a more localized absorption pattern in liver tissue.

Table 5 displays the amount of MW absorbed by liver tissue, with and without a prolate tumor, using single- and double-slot antennas at different frequencies. MW absorption (W/m³) amount increases with frequency, peaking at 2.5 GHz and 3.5 GHz for both antennas. At 3.5 GHz, the double-slot antenna performs slightly better than the single-slot antenna. Thermal damage minimizes at 3.5 GHz; despite high absorption, the energy distribution is more uniform. This helps minimize overheating in adjacent normal tissues, making it more suitable for liver treatment. The 3.5 GHz frequency with a double-slot antenna provides an optimal balance, achieving effective microwave absorption while reducing potential damage to surrounding normal cells.

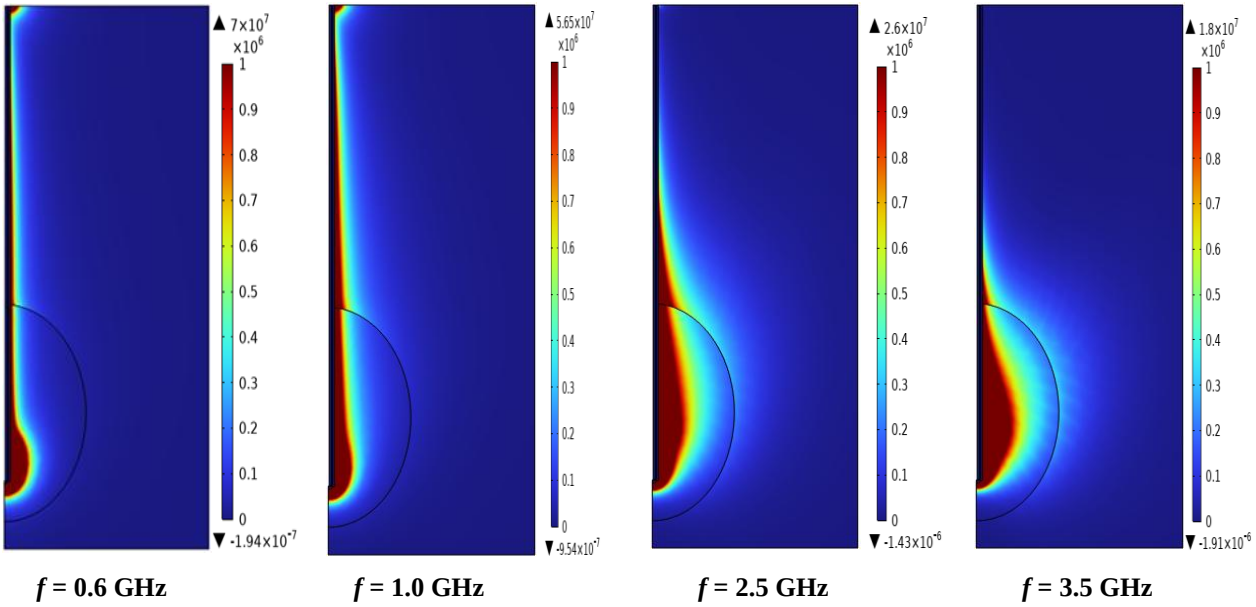

***f* = 0.6 GHz** ***f* = 1.0 GHz** ***f* = 2.5 GHz** ***f* = 3.5 GHz**

(a) Single-slot MCA

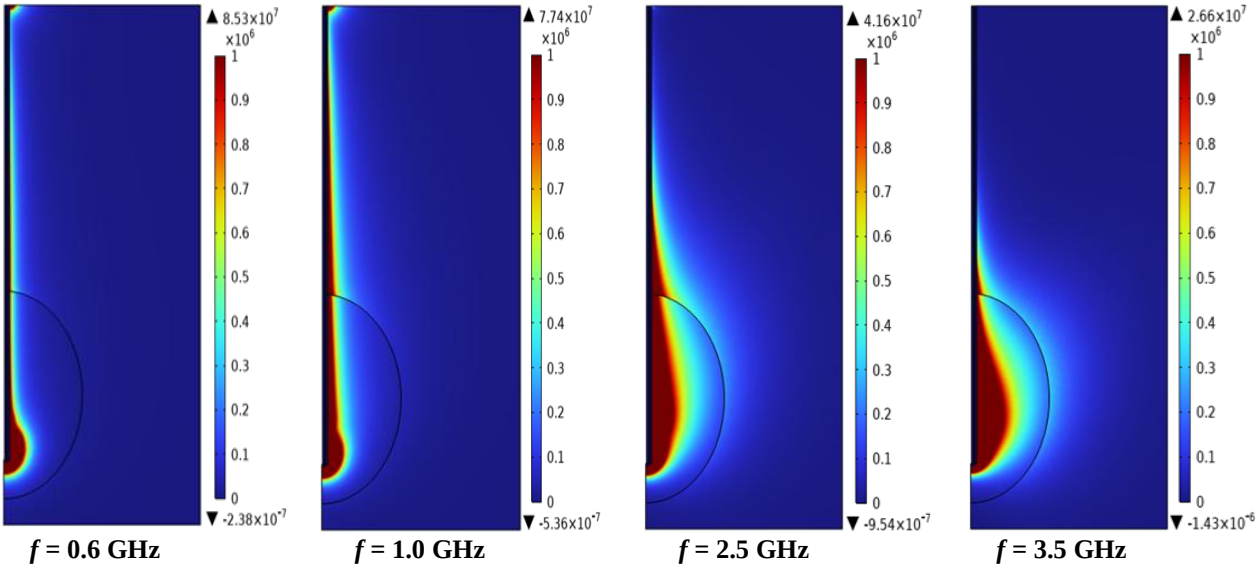

***f* = 0.6 GHz** ***f* = 1.0 GHz** ***f* = 2.5 GHz** ***f* = 3.5 GHz**

(b) Double-slot MCA

Figure 6: Total power dissipation density within a prolate tumor applying different MF using (a) single-slot, and (b) double-slot MCA with P = 12 W and t = 240 s

Table 5: MW absorbed amount by liver tissue with and without prolate tumor concerning single- and double-slot antenna for different frequencies

Microwave frequency (GHz)	MW absorption (W/m³) by liver tissue with prolate tumor		MW absorption (W/m³) by liver tissue without tumor		Observation
	Single-slot MCA	Double-slot MCA	Single-slot MCA	Double-slot MCA	
0.6	16634	11845	8817	6044.9	Lower absorption for both antennas.
1.0	28346	22671	18039	14121	Moderate absorption; the single-slot has a higher rate.
2.5	49039	48377	29938	29137	High absorption; both antennas perform similarly.
3.5	47310	48519	26377	26773	High absorption; the double-slot antenna has a slight advantage.

6.2 Role of MP on thermal damage

Microwave power (MP) is a critical factor in determining the level of thermal damage and necrotic tissue formation during the treatment of liver tumors. Selecting appropriate power settings based on tumor size, location, and composition is essential to maximize treatment effectiveness while minimizing risks and complications. Achieving the right balance between microwave power and treatment duration is crucial for optimal clinical outcomes in microwave ablation therapy for liver tumors. Figure 7(a-b) depicts the percentage of necrotic tissue in oblate and prolate tumor tissue at a frequency of 3.5 GHz and time t = 240s, due to using a single-slot antenna with varying MP.

Figure 7(a) shows the percentage of necrotic tissue within the oblate tumor. The proportion of damaged tissue increased with MP ranging from 6 to 24 W. Additionally, high microwave power led to the destruction of a significant amount of healthy tissue. The data presented in Figure 7(b) illustrate the proportion of necrotic tissue in the prolate tumor. When the input power P = 12 W and the frequency f = 3.5 GHz at time t = 240s, the damage is calculated to be 71.85% and 87.58% in the oblate and prolate tumors, respectively. This indicates that the single-slot antenna in prolate tumors causes less harm to healthy tissue compared to oblate tumors.

Thermal energy (Joules) generation in tissue results from electromagnetic wave absorption, which produces heat due to resistive losses in the tissue. Power deposition (heat source) is converted into thermal energy, thereby raising tissue temperature and facilitating the therapeutic effect. The relationship between the heat source and thermal energy is directly proportional to the input power: higher input power results in greater electromagnetic wave absorption and, subsequently, increased thermal energy. This heating effect is crucial for targeted tissue therapy, as it ensures sufficient tumor necrosis while sparing surrounding healthy tissues. Table 6 summarizes the computed thermal energy in the liver for oblate and prolate tumor geometries under single- and double-slot MCA configurations. The results indicate that double-slot MCA consistently generates slightly higher thermal energy than single-slot antennas for both tumor geometries, suggesting improved energy deposition efficiency. This highlights the potential of double-slot MCA for enhancing tumor treatment effectiveness. Oblate tumors generate significant thermal energy due to their geometric properties, which facilitate more effective electromagnetic energy confinement and absorption around the antenna region. Furthermore, oblate tumors have a larger cross-section, expanding the region where the microwave field interacts with tumor tissue, thereby increasing power deposition and heat production. On the other hand, the elongated shape of prolate tumors allows some electromagnetic energy to travel along the primary axis, resulting in lower thermal energy concentration. This shape-dependent behavior highlights the influence of tumor geometry on the distribution of microwave energy and the thermal response.

Figure 8(a-b) compares tissue damage in oblate and prolate tumor tissue when utilizing a double-slot antenna operating at a microwave frequency of f = 3.5 GHz, and time t = 240s. The double-slot antenna generates highly concentrated heat, eliminating almost 99% of malignant tissue. When applying an input MP of 12 W and an MF of 3.5 GHz for 240 seconds, the proportion of damage inside the oblate tumor is 73.43%, whereas inside the prolate tumor, it is 89.75%.

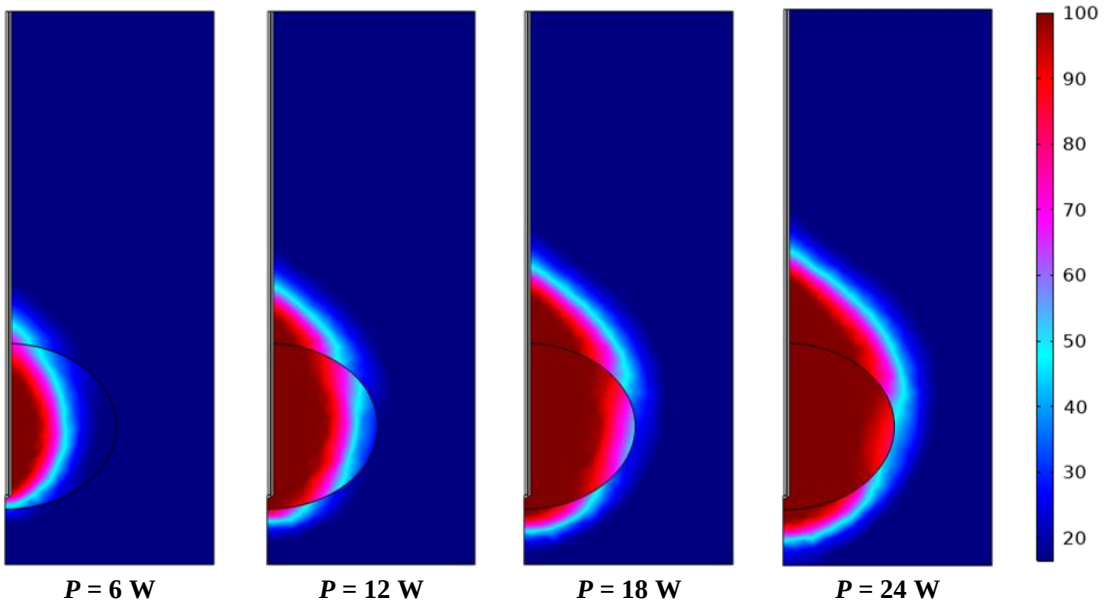

(a) **Single-slot MCA within an oblate tumor**

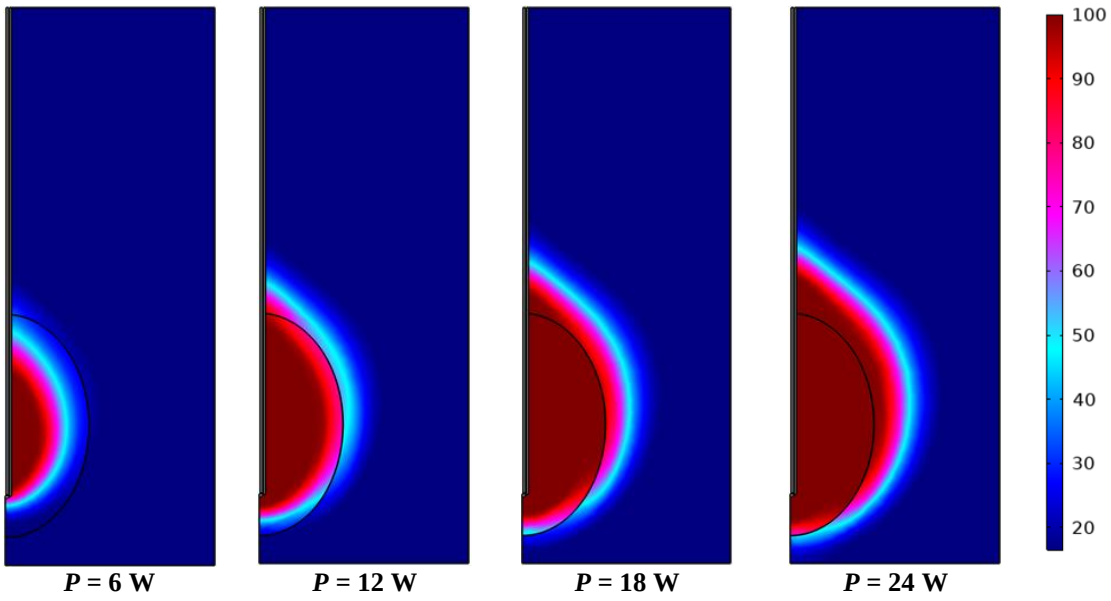

(b) Single-slot MCA within a prolate tumor

Figure 7: The proportion of necrotic tissue for MP variation using a single-slot MCA within (a) oblate and (b) prolate tumors with f = 3.5 GHz, and t = 240 s.

Table 6: Amount of thermal energy (J) generated due to various microwave powers

Microwave power (W)	Thermal energy (J) using single-slot MCA		Thermal energy (J) using double-slot MCA	
	Oblate	Prolate	Oblate	Prolate
6	1.79	1.77	1.83	1.81
12	3.51	3.48	3.59	3.55
18	5.23	5.18	5.35	5.29
24	6.96	6.89	7.12	7.04

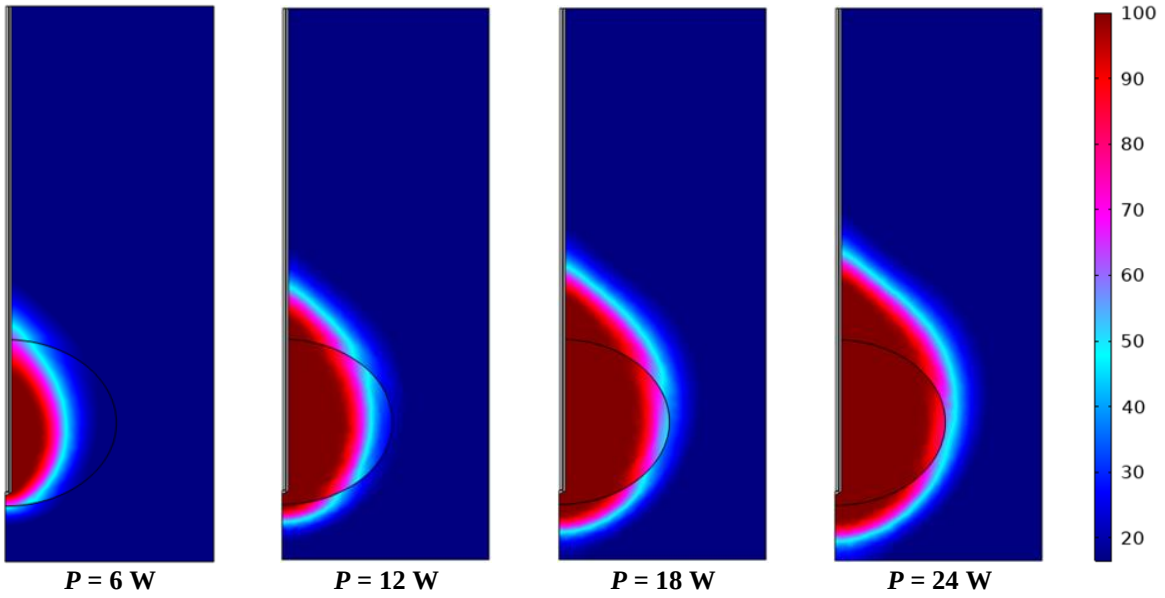

(a) Double-slot MCA within an oblate tumor

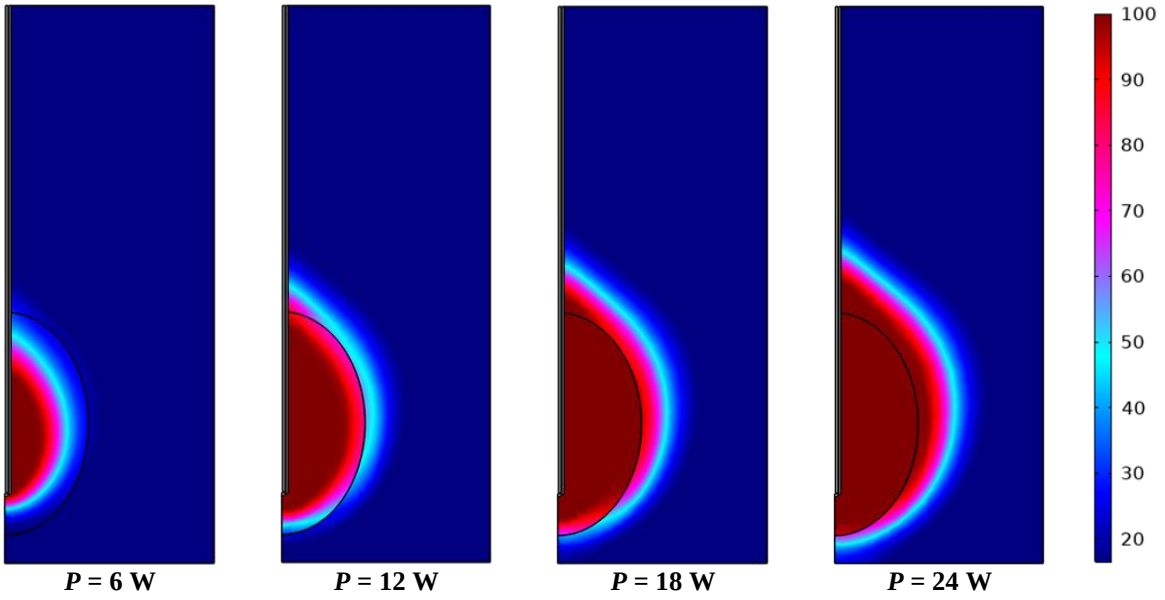

(b) Double-slot MCA within a prolate tumor

Figure 8: Fraction of necrotic tissue determined for MP variation using a double-slot antenna within (a) oblate and (b) prolate tumors with f =3.5 GHz, and t = 240 s.

Table 7: Thermal damage (%) of healthy tissue due to single- and double-slot MCA

Microwave power (W)	Thermal damage (%) of healthy tissue using single-slot MCA		Thermal damage (%) of healthy tissue using double-slot MCA	
	Oblate	Prolate	Oblate	Prolate
6	7.86	7.21	7.87	7.94
12	9.53	9.79	9.58	9.86
18	11.71	12.53	11.83	14.31
24	14.11	15.24	14.31	15.42

Table 7 illustrates the thermal damage percentages to normal tissue at various power levels (6 W, 12 W, 18 W, and 24 W) for single-slot and double-slot antennas used in treating oblate and prolate tumors. When using a double-slot antenna for oblate tumors, less damage to healthy tissue is observed than with prolate tumors. However, a significant proportion of cancerous tissue in oblate tumors remains untreated, which limits the effectiveness of this approach for smaller oblate-shaped tumors. In the case of prolate tumors, the double-slot antenna causes approximately 0.3% more damage to healthy tissue than it does for oblate tumors. Despite this slight increase in collateral damage, the double-slot antenna is notably more effective in targeting larger prolate-shaped tumors, particularly those exceeding 3–4 cm. This makes it more suitable for treating prolate tumors, where minimizing undamaged tumor tissue is critical for successful therapy.

6.3 Role of MP and MF on SAR

When assessing the effectiveness of a treatment, understanding the SAR distribution is crucial. SAR is a crucial indicator of the amount of energy biological tissues absorb from radiofrequency (RF) electromagnetic fields, such as those used in specific medical procedures, such as microwaves. Higher SAR is linked with faster tissue heating. The slot area has the greatest SAR, which diminishes with increasing distance from the slot.

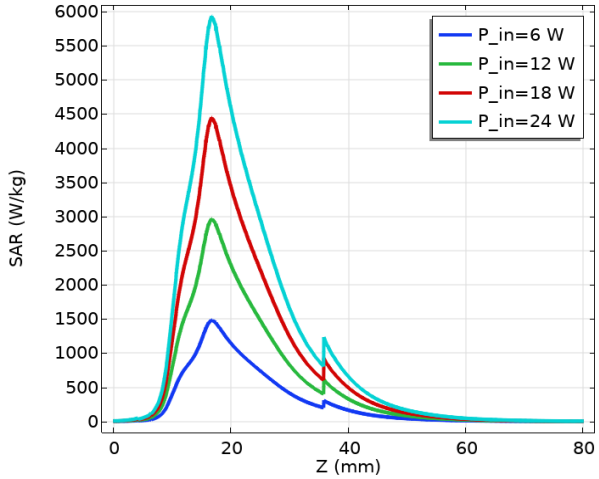

Circular tumor utilizing single-slot MCA

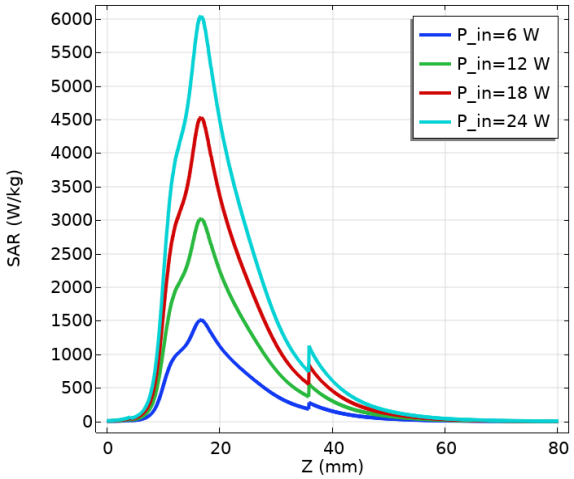

Circular tumor utilizing double-slot MCA

(a) SAR due to various input MP within the circular tumor with f = 3.5 GHz, and t = 450 s

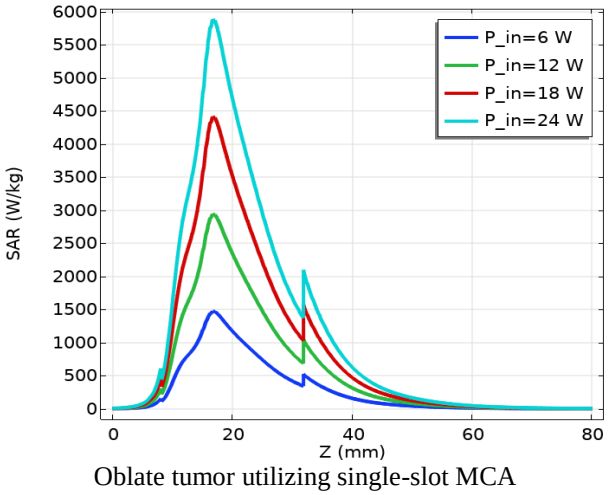

Oblate tumor utilizing single-slot MCA

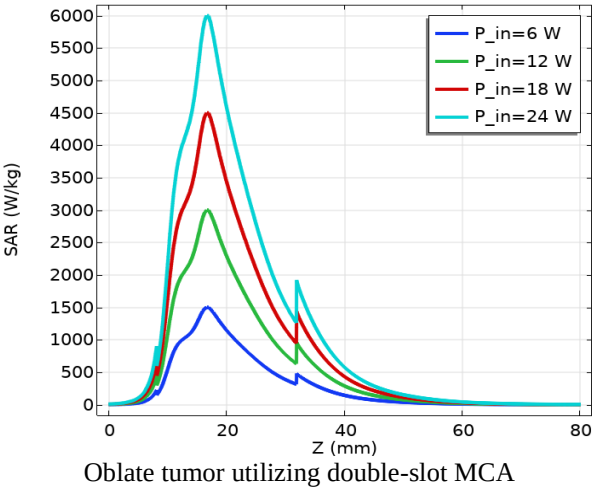

Oblate tumor utilizing double-slot MCA

(b) SAR due to various input MP within the oblate tumor with f = 3.5 GHz, and t = 450 s

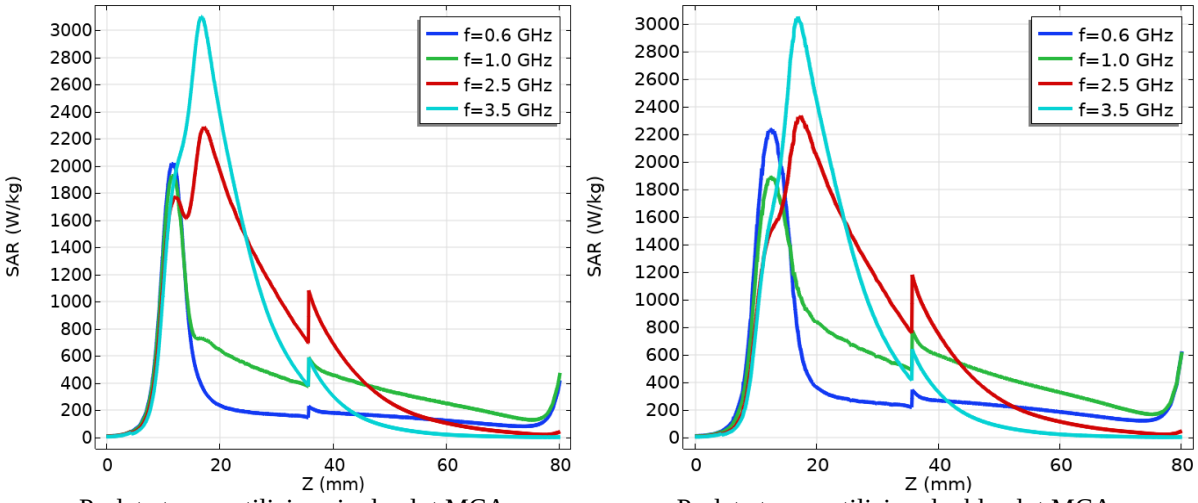

Prolate tumor utilizing single-slot MCA Prolate tumor utilizing double-slot MCA

(c) SAR due to various input MF within the prolate tumor with P = 12W, and t = 450 s

Figure 9: SAR distribution at a distance r = 2.5 mm and t = 450 s due to (a) MP using circular tumor, (b) MP within oblate tumor, and (c) MF within prolate tumor.

Figure 9(a-c) illustrates the SAR profile for a simulation duration of 450 seconds, specifically at a distance of 2.5 millimeters from the antenna axis. In Figure 9(a), we evaluate the relative merits of single- and double-slot antennas depending on different absorption rates within a circular-shaped liver tumor. We observe the highest SAR value at the maximum MP level. A single-slot MCA for 450 seconds results in a SAR of 5943.29 W/kg within the circular tumor, while a double-slot MCA results in a SAR of 6020.866 W/kg.

Figure 9(b) illustrates the SAR for different input powers (P = 6–24 W) inside an oblate tumor. Our study utilizes a frequency of f = 3.5 GHz and an ablation period of 450 seconds. When 24 W of MP is applied, the highest SAR is observed in oblate tumor tissue. The SAR rates measure 5889.88 W/kg for the single-slot antenna and 6004.54 W/kg for the double-slot antenna. It is worth noting that microwave frequency significantly influences the SAR profile.

The data in Figure 9(c) illustrate the SAR for different MF frequencies (0.6-3.5 GHz) within an elongated tumor, with a microwave power of 12 W and a heating time of 450 seconds. When employing a single-slot antenna within the tumor, the SAR at 3.5 GHz is calculated to be 3045.47 W/kg. However, when using a double-slot MCA with the same 12 W of microwave power, the SAR increases to 3099.50 W/kg. Interestingly, the liver tissue exhibits higher SAR values with the double-slot antenna than with the single-slot antenna.

The strategies employed—namely the optimization of power and frequency, the reduction of exposure time, and the enhancement of antenna design—yield effective treatment outcomes while ensuring that SAR values remain within established safety limits. Researchers should focus on implementing these methodologies within experimental frameworks and rigorously validating their safety and effectiveness in real-world applications.

6.4 Role of MF on local thermal damage

The microwave frequency (MF) is crucial for determining the extent and location of local thermal damage during the treatment of liver tumors. Higher frequencies provide more intense and localized heating, making them suitable for small or superficial tumors. Lower frequencies, on the other hand, offer deeper penetration and broader heating patterns, making them more suitable for larger tumors. Careful selection and application of the appropriate frequency, taking into account the tumor's size, location, and surrounding tissues, are essential for maximizing treatment effectiveness and minimizing risks.

Figure 10 illustrates how different MFs at different sites inside circular and oblate liver tumor tissues cause varying amounts of tissue damage throughout the ablation process. Tissue damage is observed at specific locations (r, z) = (4, 20), (8, 20), (12, 20), and (16, 20) mm inside the circular and oblate malignant tissue. This figure illustrates the pattern of tumor damage variation: The tumor necrosis progresses steadily until it reaches a saturation point, signifying the final stage of the process.

Figure 10(a) depicts the proportion of necrotic tissue in four distinct locations inside the circular tumor when using a single-slot antenna at an input power level of P = 12 W. Complete tumor necrosis is observed at the position r = 4 mm and z = 20 mm after t = 450 seconds. At the tumor boundary (16, 20 mm), with an input frequency of f = 3.5 GHz, nearly 60% of cells are damaged. This suggests that the time required for complete tumor ablation is significantly reduced when the magnetic field is very strong.

Figure 10(b) shows the necrotic tissue fraction at four points within the circular tumor when using a double-slot MCA at a power of P = 12 W. It is observed that at the boundary point (16, 20) mm, the fraction percentage of necrotic tissue is 15.03% for MF 0.6 GHz, 47.30% for MF 2.5 GHz, and 77.35% for MF 3.5 GHz at time 450s. The percentage of necrotic tissue increased with both the frequency and the ablation duration.

Figure 10(c) illustrates the proportion of necrotic tissue at four locations within the oblate tumor when employing a single-slot antenna at a certain power level of P = 12 W. The percentages of necrotic tissue fraction at the (16, 20) mm coordinate point for MF of 1.0, 2.5, and 3.5 GHz are estimated to be 20.07%, 46.74%, and 59.33%, respectively.

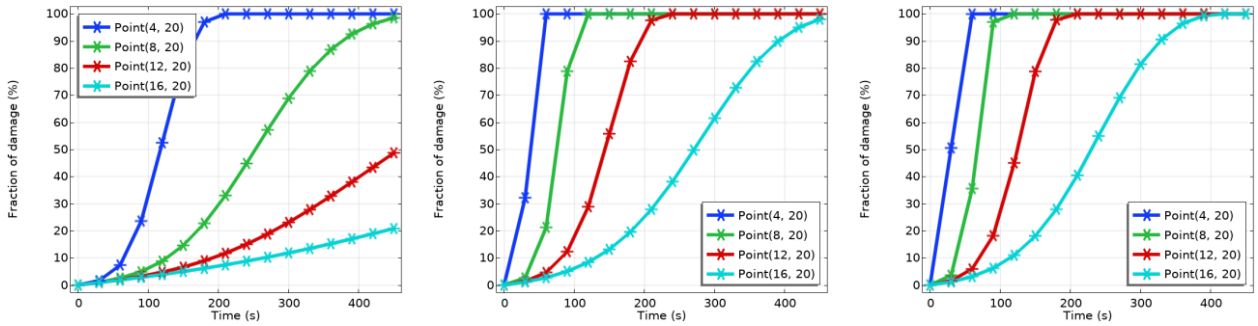

f = 0.6 GHz **f = 2.5 GHz** **f = 3.5 GHz**

(a) Necrotic tissue fraction within a circular tumor using a single-slot MCA

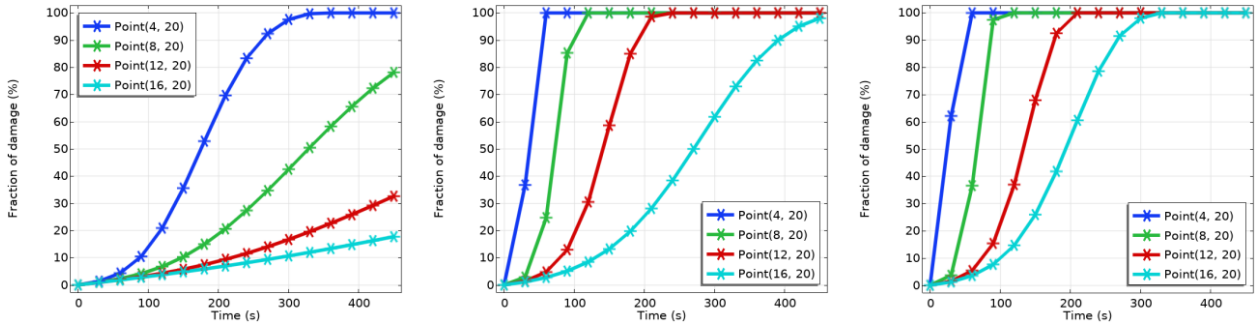

f = 0.6 GHz **f = 2.5 GHz** **f = 3.5 GHz**

(c) Necrotic tissue fraction within circular tumor using double-slot MCA

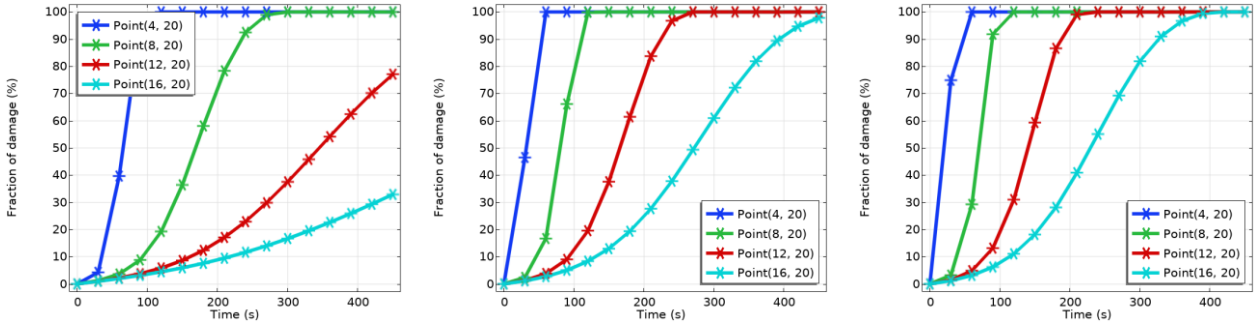

f = 1.0 GHz **f = 2.5 GHz** **f = 3.5 GHz**

(c) Necrotic tissue fraction within an oblate tumor using a single-slot MCA

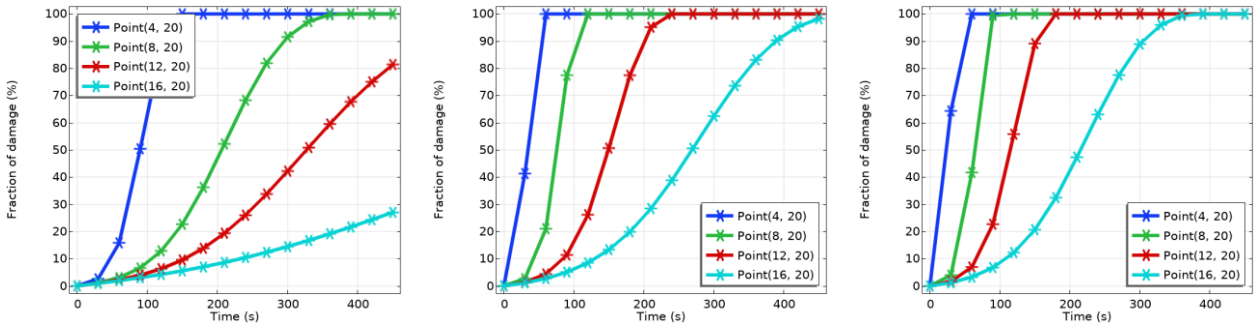

***f* = 1.0 GHz** ***f* =2.5 GHz** ***f* = 3.5 GHz**

(d) Necrotic tissue fraction within the oblate tumor using double-slot MCA

Figure 10(a-d): Within the circular and oblate tumors, necrotic tissue fraction for different MF utilizing single-slot and double-slot antennas with P = 12 W and t = 450 s.

Figure 10(d) depicts the percentage of necrotic tissue at four specific locations within the oblate tumor when a double-slot MCA is utilized at a power output of P = 12 W. At input frequencies of 1.0, 2.5, and 3.5 GHz, the estimated percentages of necrotic tissue fraction at the boundary point (16, 20) mm are 18.38%, 47.59%, and 65.62%, respectively.

6.5 Role of high-power-low-frequency and low-power-high-frequency on temperature

Figure 11 demonstrates how low-power-high-frequency and high-power-low-frequency affect the temperature distribution in prolate liver tumors. Close to the antenna slot, the temperature is at its peak and decreases as we move away from it. We analyze four locations in the prolate tumor tissue at (r, z) = (2.25, 20), (5.5, 20), (8.75, 20), and (12, 20) mm to evaluate fluctuations in the temperature profile.

Using a single-slot antenna, Figure 11(a) illustrates the distribution of temperatures throughout the prolate tumor tissue at two different input power levels: 24 W at low-frequency 0.6 GHz and 6 W at high-frequency 3.5 GHz. At time t = 450 s, temperatures at four separate locations (2.25, 20), (5.5, 20), (8.75, 20), and (12, 20) mm are 70.55℃, 59.05℃, 50.24℃, and 44.55℃ for high-power (P = 24 W) — low-frequency (f = 0.6 GHz), and 66.90℃, 57.37℃, 50.32℃, and 45.56℃ for low-power (P = 6 W) — high-frequency (f = 3.5 GHz). Notably, the temperature is slightly higher at the boundary between low-power-high-frequency and high-power-low-frequency.

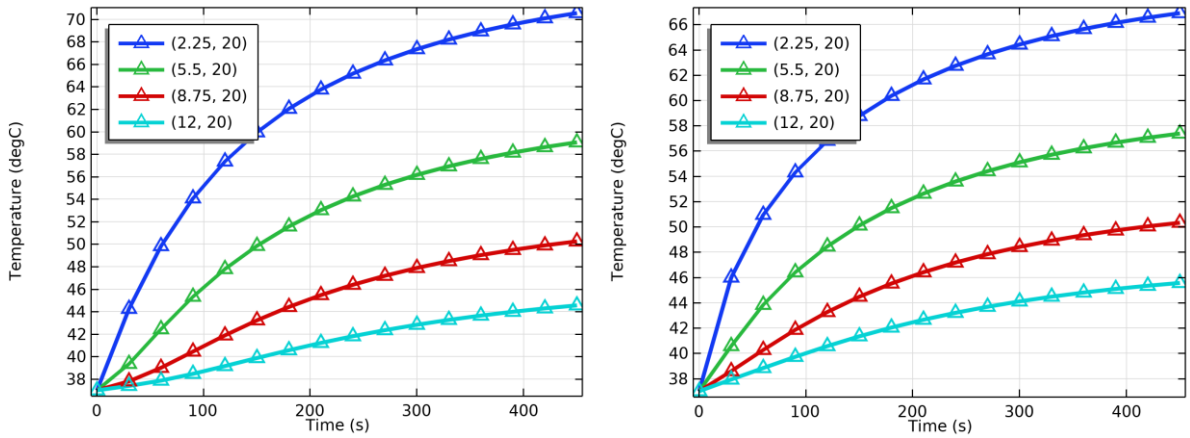

(i) Single-slot MCA (P = 24 W and f = 0.6 GHz) (ii) Single-slot MCA (P = 6 W and f = 3.5 GHz)

(a) Local temperature distribution using single-slot MCA with (i) P = 24 W and f = 0.6 GHz, and (ii) P = 6 W and f = 3.5 GHz.

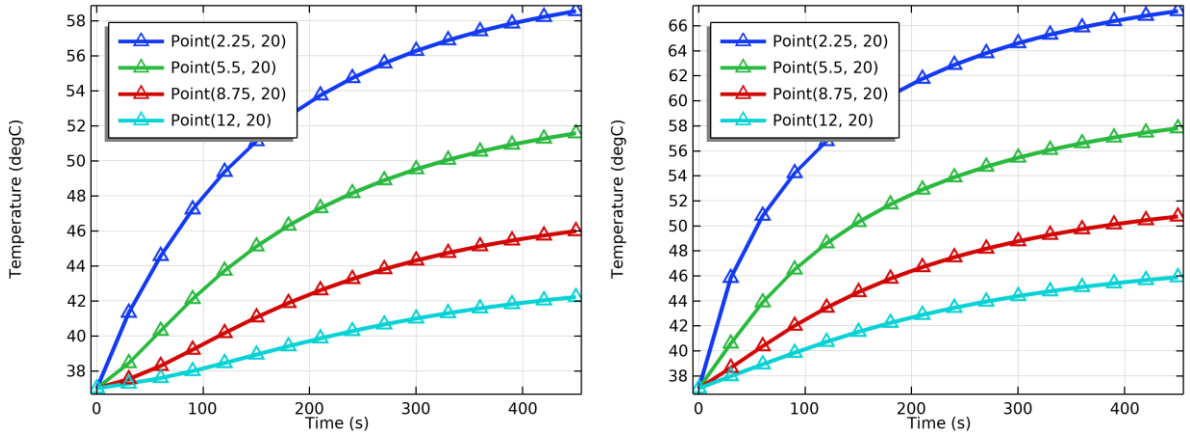

(i)Double-slot MCA (P = 24 W and f = 0.6 GHz) (ii) Double-slot MCA (P = 6 W and f = 3.5 GHz)

(b) Local temperature distribution using double-slot MCA with (i) P = 24 W and f = 0.6 GHz, and (ii) P = 6 W and f = 3.5 GHz

Figure 11: Effect of high–power–low–frequency and low–power–high–frequency on local temperature distribution at different times within prolate tumor using (a) single-slot, and (b) double-slot MCA.

In Figure 11(b), the temperature distributions within the prolate tumor tissue are visualized using a double-slot antenna. This antenna operates at both high-power (P = 24 W) and low-frequency (f = 0.6 GHz), as well as at low-power (P = 6 W) and high-frequency (f = 3.5 GHz). The estimated temperatures at four distinct points within the tumor border for the high-power-low-frequency setting are 58.55°C, 51.57°C, 45.98°C, and 42.22°C, respectively. For the low-power—high-frequency setting at the time t = 450s, the temperatures are 67.16°C, 57.79°C, 50.74°C, and 45.88°C, respectively. Notably, the double-slot MCA gradually raises the temperature inside the prolate tumor, generating more localized heat at low power and high frequency, which is essential for ablating tumors sized 3 to 5 centimeters.

Figure 12 demonstrates the effects of high-power-low-frequency and low-power-high-frequency treatments on temperature distribution across oblate hepatic tumor tissues. We investigated fluctuations in temperature profiles at four specific points within the tumor tissue, measured in millimeters: (4, 20), (8, 20), (12, 20), and (16, 20), to better understand these impacts.

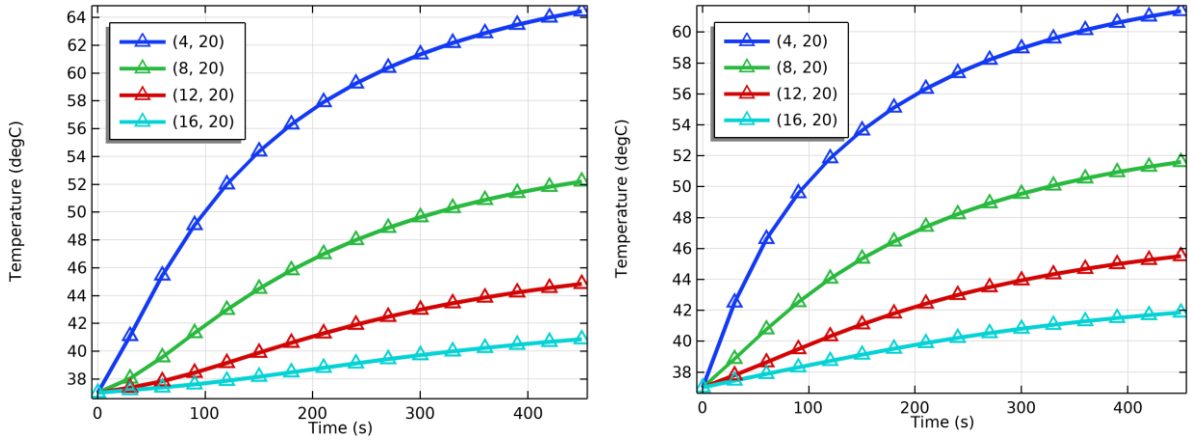

(i) Single-slot MCA (P = 24 W and f = 0.6 GHz) (ii) Single-slot MCA (P = 6 W and f = 3.5 GHz)

(a) Local temperature distribution using single-slot MCA with (i) P = 24 W, f = 0.6 GHz, and (ii) P = 6 W, f = 3.5 GHz

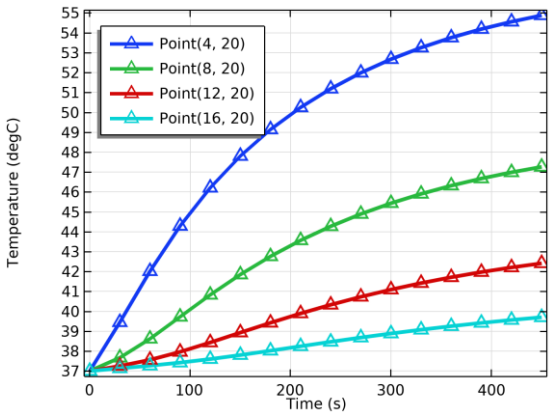

(ii) Double-slot MCA (P = 24 W and f = 0.6 GHz)

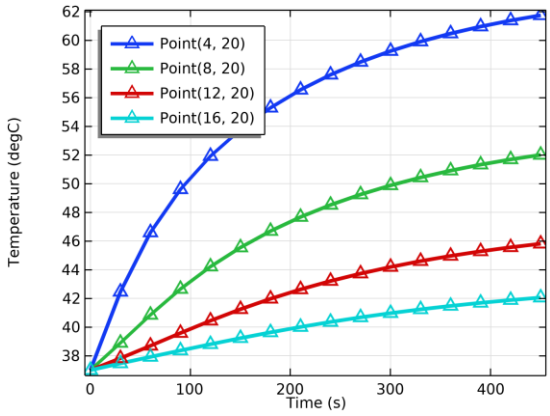

(ii) Double-slot MCA (P = 6 W and f = 3.5 GHz)

(b) Local temperature distribution using double-slot MCA with (i) P = 24 W, f = 0.6 GHz, and (ii) P = 6 W, f = 3.5 GHz

Figure 12: Effect of high-power-low-frequency and low-power-high-frequency on local temperature distribution at different times within an oblate tumor using (a) single-slot and (b) double-slot MCA.

In Figure 12(a), the temperature distribution within the oblate tumor tissue is illustrated for two scenarios: high-power (P = 24 W) and low-frequency (f = 0.6 GHz); and low-power (P = 6 W) and high-frequency (f = 3.5 GHz), achieved using a single-slot antenna. At time 450 seconds, the local temperatures at four distinct positions for low-frequency (f = 0.6 GHz) — high-power (P = 24 W) are as follows: 64.43°C, 52.19°C, 44.83°C, and 40.85°C, respectively. For low-power (P = 6 W) — high frequency (f = 3.5 GHz) the values are as follows: 61.74°C, 51.58°C, 45.49°C, and 41.84°C. The boundary-point temperature for low-power-high-frequency is marginally higher than that for high-power-low-frequency.

In Figure 12(b), the temperature distribution inside the oblate tumor tissue is depicted using a double-slot antenna. Under high-power (P = 24 W) and low-frequency (f = 0.6 GHz) conditions, the estimated temperatures at points (4, 20), (8, 20), (12, 20), and (16, 20) mm at the tumor boundary are 54.88°C, 47.26°C, 42.41°C, and 39.70°C, respectively. Conversely, at time 450s, under low-power (P = 6 W) and high-frequency (f = 3.5 GHz) conditions, the temperatures at the same points are 61.74°C, 52.01°C, 45.81°C, and 42.06°C.

6.6 Comparison

When optimizing liver tumor treatment with microwave ablation, it's crucial to consider the choice between single- and double-slot MCA carefully. Single-slot antennas provide precise, localized heating, making them suitable for smaller, well-defined tumors or tumors near critical structures. In contrast, double-slot antennas provide broader, more uniform heating, making them ideal for larger or irregularly shaped tumors and thereby enhancing the efficiency and comprehensiveness of the ablation.

In Figure 13(a), the graph illustrates the percentage of damage to malignant tissue within a prolate tumor over 60 to 300 seconds. The blue line represents the damage at the 12- and 20-mm coordinates (r, z) when using a single slot, while the red line depicts the damage caused by a double-slot MCA operating at 12 W and 3.5 GHz. Upon analyzing the line graph, it is clear that the double-slot antenna causes more damage to malignant tissue than the single-slot antenna at the border point of a prolate tumor. Between 60s and 120s, both antennas cause similar damage to the cancerous tissue. However, over time, the percentage of damaged tissue increases. At t = 300s, the single-slot antenna damaged 74.13% of the tissue, while the double-slot antenna damaged 83.27%. In prolate tumors, double-slot antennas have a lesser impact on healthy tissue and result in faster destruction of malignant tissue than single-slot antennas.

Figure 13(b) compares the proportion of damaged tissue at a specific point (16, 20) mm on the border of an oblate tumor against time using both a single-slot and a double-slot antenna. The comparison uses P = 12 W and f = 3.5 GHz. The graph illustrates that the double-slot antenna caused more damage to malignant tissue than the single-slot antenna over the specified time frame. Notably, between 60 and 120 seconds, both antennas caused similar amounts of damage to the malignant tissue. However, after approximately 210 seconds, the damage produced by the double-slot MCA increases modestly by 33.07% compared to the single-slot antenna.

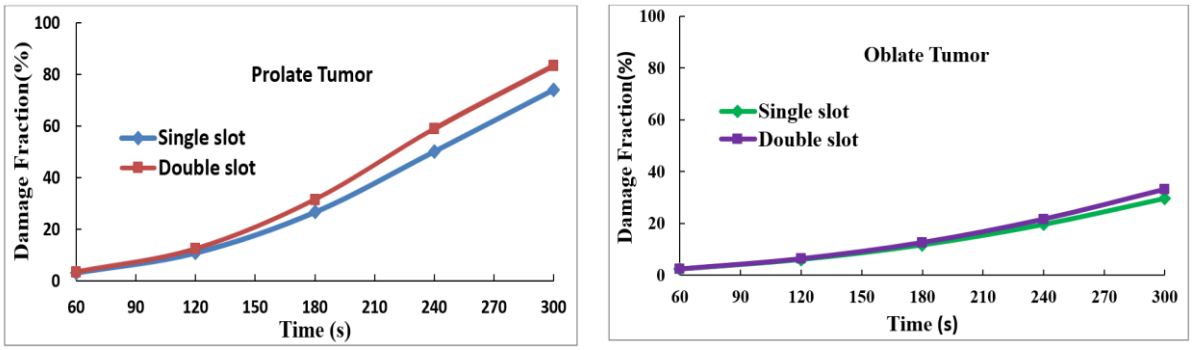

(a) (b)

Figure 13: Damage fraction (%) versus time utilizing single- and double-slot MCA attained at (a) prolate tumor border point (12, 20) mm, (b) oblate tumor border point (16, 20) mm

7. Conclusion

In the treatment of malignant tumors, microwave thermal ablation techniques have gained popularity as an alternative to other methods, such as RF ablation. In this research, we examine electromagnetic propagation and bioheat transfer for liver prolate and oblate tumors and assess single- and double-slot antennas to determine the most effective applicator for each treatment area. We evaluated the effectiveness of single- and double-slot MCA by analyzing thermal damage in the liver tumor, SAR and thermal distributions, and microwave total dissipation density. From this comparative analysis, we draw the following conclusions:

- For a certain microwave power of 12 W and microwave frequency of 3.5 GHz, it is observed that a double-slot antenna offers a more localized absorption pattern than a single-slot antenna.
- For microwave power 12 W and frequency 3.5 GHz, the percentage of average tissue damage of oblate tumor for single-slot and double-slot antennae is 71.85% and 73.43%, respectively. The percentage of average tissue damage of prolate tumors for single-slot and double-slot MCA is 87.58% and 89.75%, respectively.
- The SAR values are higher for a double-slot antenna compared to a single-slot MCA, with measurements of 6020.87 W/kg for circular tumors, 6004.54 W/kg for oblate tumors, and 3099.50 W/kg for prolate tumors. This indicates a marked difference in energy absorption between antenna designs and tumor morphologies.
- When comparing high-power-low-frequency with low-power-high-frequency within the oblate and prolate tumors, it's found that the double-slot MCA produces more localized thermal heat at low power and high frequency.

When deciding between a single-slot and double-slot MCA, it's important to consider the specific goals of the ablation procedure. This includes whether the goal is achieving high precision or covering a large volume. The selection of the appropriate antenna type should be based on the tumor's size, location, and treatment goals to maximize therapeutic efficacy and minimize risks.

Limitations

- The numerical model may assume idealized tumor shapes, but actual tumors can have irregular or varied geometries.
- Performing accurate numerical simulations can be difficult due to the need for extensive computing resources and time, which may limit the ability to explore different parameter changes.
- Conducting experimental analysis is challenging because of the lack of necessary laboratory facilities and resources.
- Assuming uniform blood perfusion in tumors oversimplifies blood flow dynamics. Tumors often exhibit heterogeneous perfusion rates due to irregular vascular structures and varying metabolic demands, which can affect the accuracy of heat transfer predictions.

Future research

- To assess the effectiveness of double-slot antennas in a broader range of clinical scenarios, researchers should expand their research to include a wider variety of tumor types and sizes.
- It is advisable to explore new materials and structural configurations to enhance the efficiency and safety of the antennas.
- To develop sophisticated tools that dynamically adjust power and frequency parameters in ablation techniques, optimizing therapy in real-time.
- The incorporation of realistic and heterogeneous blood perfusion profiles has the potential to enhance the reliability of research findings.
- To conduct an analysis using a liver tissue mimic phantom.

Competing interests

The authors state that they have no known conflicts of interest or personal ties that may have affected the work described in this study.

CRediT Author Statement

Biswas, C.: Investigation, Methodology, Mathematical modeling, Numerical simulation, Visualization, Formal analysis, Writing (original draft). **Nasrin, R.**: Supervision, Conceptualization, Validation, Writing (review and editing). **Jahan, S.**: Methodology, Writing (review and editing) **Ferdoushi, M. S.**: Formal analysis, Writing (review and editing).

References

Acikgoz, H., and Turer, I. (2014): A novel microwave coaxial slot antenna for liver tumor ablation, Advanced Electromagnetics, Vol. 3, No. 1. https://doi.org/10.7716/aem.v3i1.192

Adilakshmi, V., Akgül, A., Reddy, V. R. G., and Hassani, M. K. (2025): Thermal radiation and diffusion effects on MHD Sisko fluid flow over a nonlinearly stretchable porous sheet. Boundary Value Problems, Vol. 2025, No. 97. https://doi.org/10.1186/s13661-025-02042-6

Ali, M., Nasrin, R., and Alim, M. A., (2023): Axisymmetric boundary layer slip flow with heat transfer over an exponentially stretching bullet-shaped object: A numerical assessment, Heliyon, Vol. 9, No. 3, e13671. https://doi.org/10.1016/j.heliyon.2023.e13671

Andreozzi, A., Iasiello, M., Napoli, G., and Vanoli, G.P. (2024): Laser ablation for prostate cancer therapies: mathematical modeling. In International Symposium on Advances in Computational Heat Transfer, pp.151-162. https://doi.org/10.1615/ICHMT.2024.CHT-24.160

Betram, J.M., Yang, D., Converse M.C., Webster, J.G., and Mahvi, D.M. (2006): Antenna design for microwave hepatic ablation using an axisymmetric electromagnetic model, Biomedical Engineering Online, Vol. 5, No. 1, pp. 1-9. https://doi.org/10.1186/1475-925X-5-15

Biswas, C., Nasrin, R., and Ahamad, M. S. (2022): Numerical analogy of bioheat transfer and microwave cancer therapy for liver tissue, Heat Transfer, Vol. 51, No. 7, pp. 6403-30. https://doi.org/10.1002/htj.22597

Chang, I.A. (2010): Considerations for thermal injury analysis for RF ablation devices, The Open Biomedical Engineering Journal, Vol. 4, pp. 3-12. https://doi.org/10.2174/1874120701004020003

Curto, S., Taj-Eldin, M., Fairchild, D., and Prakash, P. (2015): Microwave ablation at 915 MHz vs 2.45 GHz: A theoretical and experimental investigation, Medical Physics, Vol. 42, No. 11, pp. 6152-61. https://doi.org/10.1118/1.4931959

Deshazer, G., Prakash, P., Merck, D., and Haemmerchi, D. (2017): Experimental measurement of microwave ablation heating pattern and comparison to computer simulations, International Journal of Hyperthermia, Vol. 33, No. 1, pp. 74-82.

Dong, F., Wu, Y., Li, W., Li, X., Zhou, J., Wang, B., and Chen, M. (2025): Advancements in microwave ablation for tumor treatment and future directions, iScience, Vol. 28, No. 4, 112175. https://doi.org/10.1016/j.isci.2025.112175

Farina, L., Nissenbaum, Y., Cavagnaro, M., and Goldberg, S.N. (2018): Tissue shrinkage in microwave thermal ablation: Comparison of three commercial devices, International Journal of Hyperthermia, Vol. 34, pp. 382-91. https://doi.org/ 10.1080/02656736.2017.1362115

Gas, P. (2018): The S11-Parameter Analysis of Multi-Slot Coaxial Antenna with Periodic Slots, Lecture Notes in Electrical Engineering, Vol. 452, pp. 367-376. https://doi.org/10.1007/978-3-319-63949-9_24

Gorman, J., Tan, W., and Abraham, J. (2022): Numerical simulation of microwave ablation in the human liver, Processes, Vol. 10, No. 2, 361. https://doi.org/10.3390/pr10020361
Guntur, S.R., Lee, K.L., Paeng, D.G., Choleman, A.J., and Choi, M.J. (2013): Temperature-dependent thermal properties of ex vivo liver undergoing thermal ablation, Ultrasound in Medicine and Biology, Vol. 39, No.10, pp. 1771-1784. https://doi.org/10.1016/j.ultrasmedbio.2013.04.014
Hossain, M. A, Nasrin, R., and Alatawi, E. S. (2025): Human skin burn intensity resulting from various incidents utilizing bioheat transfer model: A comparative analogy, Heat Transfer, pp. 1-19. https://doi.org/10.1002/htj.23291
Jiang, Y., Zhao, J., Li, W., Yang, Y., Liu, J., and Qian , Z. (2017): A coaxial slot antenna with frequency of 433 MHz for microwave ablation therapies: design, simulation, and experimental research, Medical and biological Engineering and Computing, Vol. 55, No.11, pp. 2027-36. https://doi.org/10.1007/s11517-017-1651-9
Keangin, P., Rattanadecho, P., and Wessapan, T. (2011): An analysis of heat transfers in liver tissue during microwave ablation using single and double slot antenna, International Communications in Heat Mass Transfer, Vol. 38, pp. 757-66. https://doi.org/10.1016/j.icheatmasstransfer.2011.03.027
Liu, F., Hou, B., Li, Z., Zhang, L., Zhou, Y., Bian, H., and Huo, Z. (2023): Microwave ablation of multifocal primary liver cancer guided by real-time 3.0T MRI, International Journal of Hyperthermia, Vol. 40, No. 1. https://doi.org/10.1080/02656736.2023.2228519
Lopresto, V., Pinto, R., Farina, L., and Cavagnaro, M. (2017): Microwave thermal ablation: effects of tissue properties variations on predictive models for treatment planning, Medical Engineering and Physics, Vol. 46, pp. 63-70. https://doi.org/10.1016/j.medengphy.2017.06.008
Lopresto, V., Pinto, R., Farina, L., and Cavagnaro, M. (2017): Treatment planning in microwave thermal ablation: Clinical gaps and recent research advances, International Journal of Hyperthermia, Vol. 33, pp. 83-100.
Lopresto, V., Pinto, R., Lovisolo, G.A., and Cavagnaro, M. (2012): Changes in the dielectric properties of ex vivo bovine liver during microwave thermal ablation at 2.45 GHz, Physics in Medicine and Biology, Vol. 57, No. 8, pp. 2309-2327. https://doi.org/10.1088/0031-9155/57/8/2309
Microwave Cancer Therapy, COMSOL Multiphysics Model Library 6.3.
Nasrin, R., and Sawmpa, S. A. (2024): Hepatic tumor ablation using electric current and bioheat transfer model: A 3D numerical analysis, Journal of Naval Architecture and Marine Engineering, Vol. 21, No. 1, pp. 53-66. https://doi.org/10.3329/jname.v21i1.61347
Nasrin, R., Hossain, Amzad, and Zahan, I. (2020): Blood flow analysis inside a stenotic artery using power-law fluid model, Research & Development in Material Science, Vol. 13, No. 1, pp.1360-1368. https://doi.org/10.31031/RDMS.2020.13.000803
Polychronopoulos, N. D., Gkountas, A. A., Sarris, I. E. and Spyrou, L. A. (2021): A computational study on magnetic nanoparticles hyperthermia of ellipsoidal tumors, Applied Science, Vol. 11, No. 20. https://doi.org/10.3390/app11209526
Prakash, P., Deng, G., Converse, M.C., Webster, J.C., Mahvi, D.M., and Ferris, M.C. (2008): Design optimization of a robust sleeve antenna for hematic microwave ablation, Physics in Medicine and Biology, Vol. 53, No. 4, pp. 1057-1069. https://doi.org/10.1088/0031-9155/53/4/016
Preechaphonkul, W., and Rattanadecho, P. (2022): 3D numerical analysis of focused microwave ablation for the treatment of patients with localized liver cancer embedded with a vertical and Horizontal blood vessel, Science and Technology Asia, Vol. 27, No. 3, pp. 186-203. https://doi.org/10.14456/scitechasia.2022.55
Radjenovic, M. R., Boskovic, N., Sabo, M. and Radjenovic, B. (2022): An Analysis of Microwave Ablation Parameters for Treatment of Liver Tumors from the 3D-IRCADb-01 Database, Biomedical Engineering and Materials, Vol. 10, No. 7, 1569. https://doi.org/10.3390/biomedicines10071569
Rattanadecho, P., and Keangin, P. (2013): Numerical study of heat transfer and blood flow in two-layered porous liver tissue during microwave ablation process using single and double slot antenna, International Journal of Heat and Mass Transfer, Vol. 58, No. 1-2, pp. 457-70. https://doi.org/10.1016/j.ijheatmasstransfer.2012.10.043
Reddy, V. R. G., Ganteda, C., Naseem, M., Qureshi, M. A., Jamshed, W., Eid, M. R., and Almaliki, A. H. (2025): Investigating the impact of thermal radiation, induced magnetic force, and convective boundary condition on MHD nanofluid flows, Journal of Radiation Research and Applied Sciences, Vol. 18, No. 3, 101572. https://doi.org/10.1016/j.jrras.2025.101572
Santos, I.D., Haemmerich, D., Schutt, D., Rocha, A., and Menezes, L.R. (2009): Probabilistic finite element analysis of radiofrequency liver ablation using the unscented transform, Physics in Medicine and Biology, Vol. 54, No. 3, pp. 627-640. https://doi.org/10.1088/0031-9155/54/3/010
Schepps, J.L. and Foster, K.R. (1980): The UHF and microwave dielectric properties of normal and tumor tissues: Variation in dielectric properties with tissue water content, Physics in Medicine and Biology, Vol. 25, No. 6, pp. 1149-1159. https://doi.org/10.1088/0031-9155/25/6/012

Singh, M. (2023): Modified Pennes Bioheat Equation with Heterogeneous Blood Perfusion: A newer Perspective, International Journal of Heat and Mass Transfer, Vol. 218, No. 5, 124698. https://doi.org/10.1016/j.ijheatmasstransfer.2023.124698

Singh, M., Singh T., and Soni, S. (2021): Pre-operative assessment of ablation margins for variable blood perfusion metrics in a magnetic resonance imaging based complex breast tumor anatomy: Simulation paradigms in thermal therapies, Compute Methods Programs Biomed, Vol. 198, 105781. https://doi.org/10.1016/J.CMPB.2020.105781

Sohail, M., Ali, M. H., Abodayesh, K., and Abbas, S. T. (2025): Bio-convective boundary layer flow of Maxwell nanofluid via optional homotopic procedure with radiation and Darcy-Forchheimer impacts over a stretched sheet. International Journal of Ambient Energy, Vol. 46, No. 1, 2462583. https://doi.org/10.1080/01430750.2025.2462583

Sun, Y., Cheng, Z., Dong, L., Zhang, G., Wang, Y., and Liang, P. (2012): Comparison of temperature curve and ablation zone between 915 and 2450 MHz cooled-shaft microwave antenna: Results in ex vivo porcine liver, European Journal of Radiology, Vol. 8, No. 13, pp. 553-557. https://doi.org/10.1016/j.ejrad.2011.02.013

Sung, H., Ferlay, J., Siegel, R.L., Laversanne, M., Soerjomatarm, I., Jemal, A., and Bray, F. (2020): Global cancer statistics 2020: GLOBOCAN estimates of incidence and mortality worldwide for 36 cancers in 185 countries, CA Cancer J. Clin., Vol. 71, pp. 209-249. https://doi.org/10.3322/caac.21660

Tasnim, Z.J. and Nasrin, R. (2024): Thermal wave and Pennes' models of bioheat transfer in human skin: Transient comparative analysis, Heliyon, Vol. 10, No. 21, e40109. https://doi.org/10.1016/j.heliyon.2024.e40109

Viglianti, B.L., Dewhirst, M.W., Abraham, J.P., Gorman, J.M., and Sparrow, E.M. (2014): Rationalization of thermal injury quantification methods: Application to skin burns, Burns, Vol. 40, No. 5, pp. 896-902. https://doi.org/10.1016/j.burns.2013.12.005

Wang, T., Zhao, G., and Qiu, B. (2015): Theoretical evaluation of the treatment effectiveness of a novel coaxial multi-slot antenna for conformal microwave ablation of tumors, International Journal of Heat and Mass Transfer, Vol. 90, pp. 81-91. https://doi.org/10.1016/j.ijheatmasstransfer.2015.06.030

Waseem, F., Sohail, M., Lone, S. A., and Chambashi, G. (2023): Numerical simulations of heat generation, thermal radiation and thermal transport in water-based nanoparticles: OHAM study, Scientific Reports, Vol. 13, No. 1, 15650. https://doi.org/10.1038/s41598-023-42582-4

Wu X., Liu, B., and Xu, B. (2016): Theoretical evaluation of high frequency microwave ablation applied in cancer therapy, Applied Thermal Engineering, Vol. 107, pp. 501-07. https://doi.org/10.1016/j.applthermaleng.2016.07.010

Yang, D., Converse, M.C., Mahvi, D.M., and Webster, J.G. (2007): Expanding the bioheat equation to include tissue internal water evaporation during heating, IEEE Transactions on Bio-medical Engineering, Vol. 54, No. 8, pp. 1382-1388. https://doi.org/10.1109/tbme.2007.890740